Master Thesis

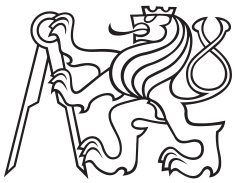

Czech Technical University in Prague

F3

Faculty of Electrical Engineering
Department of Cybernetics

# Extracting Material Properties of Objects from Haptic Exploration Using Multiple Robotic Grippers

**Bc. Pavel Stoudek**

**Supervisor: Mgr. Matěj Hoffmann, Ph.D.**
**Supervisor–specialist: Mgr. Karla Štěpánová, Ph.D.**
**Field of study: Cybernetics and Robotics**
**Subfield: Robotics**
**May 2020**

# Acknowledgements

I would like to thank Matěj Hoffmann for his guidance, Karla Štěpánová for her helpful advice, Hynek Chlup for his valuable insights into material properties, my family and friends for their never-ending support.


# Declaration

I declare that the presented work was developed independently and that I have listed all sources of information used within it in accordance with the methodical instructions for observing the ethical principles in the preparation of university theses.

Prague, May, 2020

Prohlašuji, že jsem předloženou práci vypracoval samostatně a že jsem uvedl veškeré použité informační zdroje v souladu s Metodickým pokynem o dodržování etických principů při přípravě vysokoškolských závěrečných prací.

V Praze, květen 2020

# Abstract

In this thesis, three different robotic grippers (the OnRobot RG6, Robotiq 2F-85 and the qb SoftHand Research) are utilized for haptic exploration of material properties of various objects. The Robotiq FT 300 force/torque sensor is also used to extend the scope of the measurements and as a comparison to the grippers. The feedback of the grippers is accessed and material characteristics like stiffness and elasticity are investigated through controlled squeezing. Two datasets of total of 27 objects were created and measured. The first dataset contains 20 polyurethane foam blocks; the second consists of 4 dice and 3 cubes. For this, the feedback possibilities of the grippers were investigated and measuring routines in ROS were implemented. The data are processed and transformed into a relation of stress and strain. The Young modulus of the materials is computed. The results are presented in the form of graphs so the relation can be clearly observed and compared among the individual grippers. The sorted Young moduli for each set are included. From the relations of stress and strain, the material elasticity can be evaluated. The objects exhibit nonlinear properties but the relations generally correspond to the compression stress values stated by the manufacturer. However, it is problematic to determine the Young's modulus accurately.



**Keywords:** Haptic exploration, Robotic grippers, Stiffness estimation, Force feedback, Squeezing action, Soft objects, Deformable objects

**Supervisor:** Mgr. Matěj Hoffmann, Ph.D.



# Abstrakt

Tato práce popisuje využití 3 robotických uchopovačů (OnRobot RG6, Robotiq 2F-85 a qb SoftHand Research) k haptickému průzkumu vlastností materiálu různých objektů. Také byl využit Robotiq FT300 force/torque senzor k rozšíření měření a pro porovnání s ostatními uchopovači. Díky výstupu senzorů jednotlivých uchopovačů můžeme vyšetřit vlastnosti materiálů jako pevnost a pružnost. Vyšetřování probíhá kontrolovaným mačkáním materiálu. Byly vytvořeny a změřeny dva sety předmětů obsahující celkem 27 objektů. První set obsahuje 20 bloků z polyuretanové pěny různých vlastností, druhý set je tvořen 7 kostkami různých rozměrů a materiálů. Po seznámení se s možnostmi jednotlivých uchopovačů byl pro automatizaci měření použit systém ROS, ve kterém byly implementovány algoritmy pro řízení měření a sběru dat. Získaná data byla po zpracování převedena na vztah napětí a deformace. Také byl vypočítán Youngův modul pružnosti. Výsledky jsou zobrazeny ve formě grafů a závislosti jednotlivých materiálů mohou být porovnány mezi uchopovači. Seřazené modely pružnosti pro každý set jsou uvedeny v příslušných tabulkách. Ze závislosti napětí a deformace lze určit pevnost materiálů. Měřené objekty projevují nelineární vlastnosti, ale průběhy poměrně odpovídají vlastnostem udávaných výrobcem. Nelineární vlastnosti ale komplikují přesné určení modulu pružnosti.



**Klíčová slova:** Haptický průzkum, Robotické uchopovače, Určování pevnosti, Mačkání předmětů, Měkké přeměty, Deformovatelné objekty

**Překlad názvu:** Získání vlastností materiálu skrze haptický průzkum pomocí různých robotických uchopovačů

# Contents

# Chapter 1

# Introduction

The sense of touch is crucial for many human tasks and to automate such tasks, robots will need to utilize not only vision but also haptic sensing. Nowadays, many promising tactile sensors for robots are being developed, but the interpretation of their signals is still not fully exploited [1]. Compared to robotic vision, which is able to guide us to the pre-grasping position, force and tactile sensors provide a continuous flow of sensory data also during the grasping of the object, which allows more sensitive adjustments of the grasp, leading to better manipulation with the object (dexterity of manipulation). Therefore, these sensors allow us to explore material properties such as stiffness or elasticity, thus further improving our ability to handle the given object. This is critical especially for deformable objects [2].

For us humans, the sense of touch is provided by the nerve endings and touch receptors in our skin. This is called a somatosensory system and is responsible for every impulse we feel. This way we can learn the information about the outside environment through our skin. We can feel the pressure, temperature, texture, vibrations and even pain [3]. As excellent as this natural system is, we cannot yet fully utilize a similar approach for the robot (even though there exist several artificial skin research works (e.g. [4], [5], [6])). One then must look for a different solution.

We, humans, mainly use these receptors to get the haptic feedback when interacting (touching, grasping, stroking, ...) with the world around us. However, the robot must get the desired feedback differently. Thankfully, for the task of grasping objects there exist various robotic grippers equipped with sensors that can provide the information which can be interpreted as a sense of touch. Unfortunately, these specialized grippers are often very expensive, hard to obtain, difficult to work with or they need other special equipment. Surely, there must be a simpler way to give the robot a sense of touch, which we attempt to find.

Therefore, the main goal of this thesis is to extract material properties of various object datasets using haptic exploration with multiple robotic grippers. Standard industrial grippers are used for this purpose. These can be found in a pick & place setups and can be considered (for robotic standards) fairly cheap and obtainable. This research was performed in the context of the European project IPALM [7].

## 1.1 Problem statement and proposed solution

The aim of this research was to explore material stiffness and elasticity of individual objects via controlled grasping by several industrial grippers. We strived to gather as much of the feedback data as possible, exploring various gripper configurations and speeds. During the research following robotic arms and grippers were used:

- the Universal Robots UR10e with the OnRobot RG6 gripper
- the Kinova Gen3 with the Robotiq 2F-85 gripper
- the QB Soft Hand Research

to explore different objects of various shapes and stiffness. As a reference, the Robotiq FT 300 force/torque sensor is used; the measurements from this sensor are attached in the results for a comparison. The Festo adaptive shape gripper DHEF is also mentioned, as an example of a device not well suited for this research. The possibilities of the individual robotic setups were explored, grasping routines were implemented together with the supporting scripts for the data analysis. The whole time consuming process was documented for future users. Data from proprioceptive and force feedback were collected. All the used grippers are not predisposed for providing haptic feedback: they are not equipped with tactile sensors and the available sensors do not have a good precision nor resolution. However, an attempt was made to overcome this fact.

The approach to solve the above-stated problem consisted of several stages. To enable comparison of results from multiple setups

1. 2 sets of objects with a focus on soft/deformable materials were created;
2. reference values for the datasets from technical data sheets and force/-torque sensor measurements were obtained;
3. material stiffness and elasticity was explored through various grasping/squeezing on each experimental setup;
4. relation of force and object compression was explored;
5. transformation of the feedback data to physical quantities/units was attempted.

This enabled the evaluation of individual setups limitations and their ability to identify material properties of measured objects. Moreover, the object datasets will be used to extend standard YCB dataset [8].

## 1.2 Organisation of the thesis

This document is divided into several chapters. Chapter 2 presents the related work, state of the art and technological background. Chapter 3 describes

in detail the experimental setups used, introduces the robotic manipulators and grippers. The software settings and the implementation of the gripping algorithms is described. Background of the Young's modulus is also mentioned. Chapter 4 contains the information about the material datasets and performed experiments for each setup. The results in the form of graphs are presented and interpreted in this chapter as well. Chapter 5 is the conclusion. Chapter 6 discusses the results and future work.

# Chapter 2

# Related work

In this chapter a brief literature review concerning mainly tactile perception, robotic grippers and touch sensors is presented.

## 2.1 Tactile perception and haptic exploration

### 2.1.1 Definition

Authors of [9] define tactile perception as *the process of interpreting and representing touch sensing information to observe object properties.* Unlike computer vision, this kind of perception does not have to cope with input variations like occlusions, scale and lighting condition. With this method, robot can manipulate the object to find non-visible information without the need of giant training datasets [10]. In [9], tactile sensors are categorized in 3 categories as follows:

- Single-point contact sensors – corresponding to a single tactile cell;
- High spatial resolution tactile arrays – corresponding to a human fingertip;
- Large-area tactile sensors – corresponding to a large surface of human skin.

*Representations of tactile data are commonly either inspired by machine vision feature descriptors, where each tactile element is treated as an image pixel, biologically inspired, or resort to dimensionality reduction* [9]. For object classification the object texture and stiffness are the most valid characteristics. In this work the object stiffness is the most important parameter and we deal with the first category as the used grippers can be assumed analogous to a 1 tactile cell. Haptic exploration is defined by [11] as *purposive action patterns that perceivers execute in order to encode properties of surfaces and objects, patterns that are executed spontaneously and also appear to optimize information uptake.* In [11] exploratory procedures are specified as follows:

1. Lateral motion – explores the surface texture;

2. Pressure – explores the compliance or hardness;
3. Static contact – explores the apparent temperature;
4. Unsupported holding – explores the weight;
5. Enclosure – explores the global shape, size;
6. Contour following – explores the exact shape.

For our purposes, items 2 and 5 are the most important. However, all of the above can be implemented for the use in robotics.

### 2.1.2 Relevant research

#### Exploring the object deformation

Authors of [12] discuss the way to decide the characteristics of deformable objects using a robot arm equipped with a force sensor. The force is observed as well as the object deformation by a depth camera. The method can also predict the deformation. The Young's modulus and Poisson's ratio are used to describe the object properties. The arm with the force sensor is pushing into an object, gradually increasing the force, up to a maximum of 50 N. The depth camera is observing the movement of the surface points. Soft objects like a foam cube, plush toy or a balloon were tested. The outcomes of this research are then extended in [13] and used for robot navigation purposes. The robot is touching the world around it and measures the relation between a force and deformation. The method is successfully used for navigating through deformable objects like curtains or vegetation.

Very similar are robotic surgical systems. A method for categorizing mechanical characteristics of a soft skin during robotic surgical manipulation is discussed in [14]. Using a force sensor and a stereo camera setup to record the robotic arm manipulating the skin. Young's modulus and Poisson's ratio were used for describing the measured properties. After simulating the process, the experiments validated the method on silicon rubber skin with known parameters (some experimentally measured). The robot repeatedly stretched and released the material, in some occasions it was also twisted. The camera recorded marks on the skin and thus could observe the deformation. The method also works for irregular shaped objects and the results are very close to the manufacturer's values and experimentally measured data.

In [15] two robotic arms, using common silverware can, recognize properties of basic food. The various food including fruit and vegetable is divided into 12 categories and made into a dataset of 941 instances. The robot uses specific motions and specific combinations of forks and knives to test for the specific characteristic. The hardness, plasticity, elasticity and other properties can be determined. To present its capability, the robot can prepare a bowl of salad.

### Exploring the surface texture

Authors of [16] use a uSkin tactile sensor in tandem with a web camera to stroke a material to obtain the measurement data. They can connect the outputs from both sensors to feed it to an encoder-decoder network to train it. The network can then be used to predict a type of material based on an image of its surface. It can predict material characteristics like softness or roughness and friction.

Another robot using a tactile skin for classifying various materials is presented in [17]. Deep learning network is used to recognize objects from a dataset of 36 materials with an accuracy of 95 %. A performances of a human and a robot were compared. The robot is equipped with a tactile skin on its fingertip, the finger is then swept over the object surface. The materials include leather, various fabrics, rubber, foams, wood as well as metal. The TactNet neural network was extended, so it can recognize the all of the materials.

In [18] vibrations emerging from an object when moving an accelerometer sensor on its surface are measured. The output of the sensor can then be used for the object texture recognition and classification. Amount of 43 textures like brick, paper, various foams, fabrics, wood and the like are made into a database of recordings.

### Classification based on tactile sensing

In [19] deep neural network model was used for a material classification. The model is able to process large amount of data as the touch sensors output large data sequences. The classifier was used in two kinds of setups. A 6-Legged robot equipped with a force/torque sensor on its front legs, trying to discriminate between sand, gravel, concrete, rubber and other possible terrain materials. Other a fingertip-like device using an optical force sensor, mounted on a robotic arm. The maximum measured force was 25 N and everyday objects were measured, each described by Young's modulus and ultimate tensile strength. The touch classification of the objects is more precise (the system achieved 100 % accuracy on the dataset) than that of the surface materials (98 % accuracy), as those are less homogeneous, and the structure can vary more.

Neural networks are often used for haptic object categorization. According to [20], 3 neural models were used for classification of 16 objects. The robot used in this case is a humanoid robot NICO that can provide feedback from multiple sensors. Over 80 thousand measurements were gathered and then used for a training dataset. The best model can classify every 2 out of 3 objects.

In [21] a quadruped robot with multiple sensors like accelerometers, pressure sensors and joint potentiometers is used to classify the surface underneath him. One variant of the robot also has an inertial measurement unit. The robots perform various movements on various surfaces. The same is also performed in a simulation. The SVM classifier can distinguish between the

surfaces with accuracy of over 90 % and approaching 100 % when classifying for every movement separately.

Using tactile skin on the forearm of the robotic arm for object identification in the robot's surroundings is described in [22]. The sensor output is recorded over a time period. The goal was to decide whether the object is soft or otherwise and whether the object is movable or not. The k-NN classifier was utilized to classify an approached object from the set of 18.

Spiers, Adam J., et al. [23] present two fingered gripper equipped with barometric touch sensors on its fingers. The emphasis was put on finding an affordable solution. The sensors measure the pressure when touching everyday objects and also ones from a custom made set (cylinders and rectangles of varying stiffness, same shape, different size). The team also used the YCB dataset [8]. Unlike others they hadn't used the Young's modulus as the position change could not be determined. The random forests classifier was used

Haptic sense is crucial in a robot-human interaction as the robot must not harm the human user. Authors of [24] use an SVM classifier to distinguish between a human hand or a solid object. The two-jaw gripper is equipped with pressure sensors and a dataset of measurements is used to train the classifier. The presented classifier has a 99 % accuracy.

Another of the applications where object classification based on tactile sensing can be greatly appreciated is sorting waste for recycling purposes. Chin, et al. [25] state, that manual recycling is demanding and assiduous work that can benefit greatly from the introduction of robotic object classifier. In their work, they present a special two fingered hand that can grasp even sharp objects, that would be harmful for a normal robot. The hand is equipped with pressure and strain sensors and, utilizing linear classifier, can distinguish between plastic, paper and metal objects.

## 2.2 Robotic grippers and touch sensors

In this section a basic categorization of robotic grippers and touch sensors is described as the type of the gripper and sensors it is equipped with defines which material properties can be explored and how. Selected research works are presented.

### 2.2.1 Robotic grippers

This subsection is dedicated to robotic grippers as standard industrial grippers were used for the material exploration.

#### Categorization of robotic grippers

In [26] the robotic grippers are categorized based on their configuration, actuation, size, stiffness and application. Based on the gripper configuration,

mostly 2-finger grippers were used in this work . These grippers are servo-electric in terms of actuation, regular sized, with rigid joints and links and intended for industrial applications. According to [26], the actuator for the fingers is an electric motor, that offers simple control, flexibility and doesn't require extensive care in terms of service. This also results in a lower cost. The disadvantage of the electric motor is a limited gripping force. Being for industrial purposes means the gripper is developed robustly and with sufficient precision.

Next type of gripper relevant for this work is an anthropomorphic 5-finger robotic hand that is cable-driven, human-sized, soft and suitable for research purposes. In this case, the single electric motor moves all the fingers via cables. The soft, adaptable character of the gripper fingers allows to grasp a large variety of differently shaped objects without damaging them.

The last type of robotic manipulator that might be of interest is a flexible ball gripper, which is vacuum actuated, soft and for industrial purposes. These grippers work on a principle of a rubber surface deforming after air is sucked out of them. This way the rubber body of the gripper constricts about the grasped object and the vacuum inside the gripper holds the object in place.

### 2.2.2 Touch sensors

Tactile properties are usually explored with the use of touch sensors. Research work that is related to the topic of the thesis is mentioned. Works addressing the development of devices that could be useful for this kind of research are also mentioned. Moreover, most used sensors in tactile perception are briefly described.

#### Touch sensors categorization

The most common touch sensors mentioned in [27] are:

- Piezoresistive sensors;
- Capacitive sensors;
- Piezoelectric sensors.

Piezoresistive effect describes a relation of material resistance and mechanical deformation of the said material. The resistance changes when a mechanical force is applied. This property is used in force sensing resistors, pressure-sensitive rubber and piezoresistive fabrics. According to [27], this kind of sensors is simple to manufacture and can be used in flexible setups. The disadvantage is that these sensors can be affected by a change of temperature, they have a non-linear response and hysteresis and a permanent deformation can occur.

Capacitive sensors are formed by two electric conductors in the form of metallic plates with a dielectric material in between them. When pressing on

the sensor, the dielectric material compresses and the capacitance is changed. The advantage is higher frequency response in comparison to piezoresistive sensors as mentioned in [27]. The disadvantages are similar to piezoresistive sensors. The capacitive sensors are also prone to electro-magnetic noise.

Piezoelectric effect is simply an accumulation of electric charge in the crystalline material when mechanical force is applied to the surface of the crystal. For tactile sensors a polyvinylidene fluoride film strips coverd with rubber are used [27]. The strips are chemically stable and flexible. The advantage is higher frequency response in comparison to both previously mentioned sensors. The disadvantage is sensitivity to temperature changes and application only for dynamic measurements.

### 2.2.3 Relevant research

The importance of an adequate sensor in tactile sensing is obvious. In [28] a touch rubber skin utilizing piezoresistive sensor array is introduced. This skin is very elastic and can be placed on the jaws of the gripper. By squeezing various objects and then employing a k-nearest neighbour classifier the authors were able to successfully distinguish between the objects.

The usage of the piezoresistive sensors is quite common and can be embedded into a whole new soft robotic manipulator. The gripper described in [29] is equipped with five tactile sensors and a curvature sensor. Therefore, it can be used to get haptic feedback. Similarly, in [30], where each finger uses a resistive bend sensor, so a curvature of each finger can be decided. This is then used for classification of solid objects based on their diameter. A k-nearest neighbours classifier is utilized.

Team in [31] utilized a JPL/Standford robot hand that offers many measuring possibilities. Using sensors in the wrist of the hand to measure forces and torques, likewise measuring torques in the finger joints and finally using tactile arrays on the fingertips enabled gathering a very extensive haptic information when manipulating the object. This ability was used for measuring a wide variety of objects and characteristics like hardness, plasticity and elasticity could be classified.

A robotic hand in [30] is equipped with strain sensors on the fingertips and in the palm of the hand as well as angle sensors in all the joints. This anthropomorphic robot hand can thus investigate different objects. It is capable to squeeze and tap the objects. Characteristics like softness and surface roughness can be determined. It can successfully distinguish between 7 different materials.

Another anthropomorphic hand presented in [32] utilizes the skin with resistive touch sensors. Each finger is also equipped with a special movable fingertip. These fingertips have 2 potentiometers that can measure the movement in 2 axes, therefore providing extra degrees of freedom and extending the received haptic information. The hand is then used in a series of different grasps and the gathered haptic data are used together with the finger positions for the object classification.

# Chapter 3

# Experimental setup and methods

In this chapter used experimental setups are described, specific processes and used methods are presented. For convenience, the following text is organised into sections, each focusing on a single robotic setup. Each section is then split into subsections describing the hardware, software and other unique characteristics depending on the specific setup. The necessary physics theory of stiffness and elasticity encountered during the experiments is also presented as well as the principle of supporting MATLAB functions.

In short, the procedure is very similar for every setup. the documentation was studied for every robot and the gripper, a method for the object gripping was devised, a ROS control set up, a program implemented, data from the gripping of the objects collected, modified and finally the results were plotted in MATLAB. The results were then analyzed, evaluated and a Young modulus for each object was determined. The familiarization with the robotic setups was not straight forward. For all the robots, the information was gathered from various sources and custom functions and scripts had to be implemented. This was all documented for other users interested in the project. This chapter therefore describes the gained experience with the setups. All the code used in this thesis is available at the dedicated Gitlab online repository [33].

## 3.1 UR10e with the OnRobot RG6 gripper

First, we started working with the UR10e collaborative robot. The UR10e was equipped with the OnRobot RG6 gripper. Two main control options for the robot are the Polyscope interface on the teach pendant, which utilizes so called URCaps, and the URScript, which is a Python like script that offers basic functions to operate the robot. The intent from the beginning to control the robot and the gripper through ROS and C++ programming language proved to be quite difficult to implement and therefore a different route had been chosen and a script that controls the gripper and sends the results to the PC through a TCP socket connection was made.

### 3.1.1 Hardware

#### UR10e manipulator

The UR10e is a 6 DOF collaborative industrial robot from the Universal Robots e-series with a payload of 10 kg [34]. It includes a control box that is connected to the teach pendant with a Polyscope OS and to the installed emergency button. This box can be also connected to the local laboratory network via an Ethernet cable. The manufacturer puts emphasis on the Polyscope control of the robot on the teach pendant via supplied URCaps and code snippets. The robot setup, installation, Polyscope control and functions are described in [35]. This robot unit is also equipped with an Airskin protective kit.

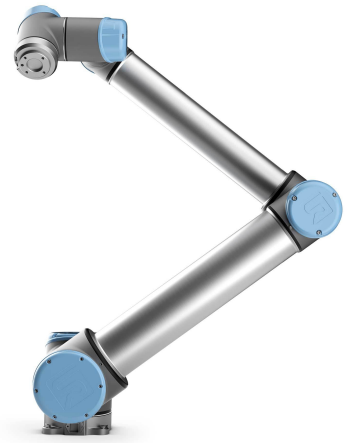

**Figure 3.1:** The Universal Robots UR10e robot [36].

#### OnRobot RG6 gripper

The OnRobot RG6 is a flexible collaborative gripper with a 160 mm stroke, easily changeable finger tips, adjustable force and gripper status feedback (digital and analog) [37]. The gripper is provided with its own URCap, that must be installed to the Polyscope OS of the robot, which is simple and straightforward. The URCap can be then used for a simple control of the gripper from the teach pendant. However, this solution lacks the more elaborate control support which was required. Therefore, a more complex approach was chosen and it is described further in the software section (see Section 3.1.2). The gripper fingertip dimensions are shown in Figure 3.2b, to compute the surface area the fingertip shape is divided into a rectangle of $25 \times 26$ mm and to a half of the ellipse with semi-major axis of 12.5 mm and semi-minor axis of 11 mm. The total surface area is thus 866 $mm^2$, this is useful for pressure and Young modulus calculations. Additional information is described in the gripper data sheet [38]. The gripper is connected to the robot (and to its control box) by a cable with a 8-pin connector (type

**(a) :** The OnRobot RG6 gripper [39].

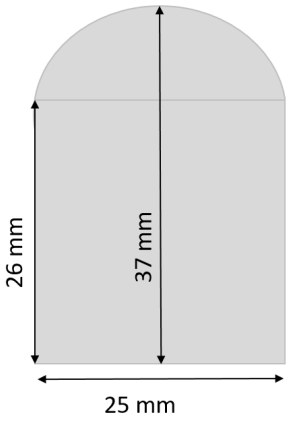


**(b) :** The OnRobot RG6 gripper fingertip dimensions.

SAC-8P-PUR), the pinout is as shown in the Figure 3.3. For our purposes

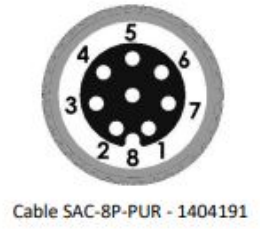


| pin | wire | UR I/O | UR I/O V3 |
|---|---|---|---|
| 1 | White | AI2 | Tool analog input 2 |
| 2 | Brown | AI3 | Tool analog input 3 |
| 3 | Green | DI9 | Tool input 1 |
| 4 | Yellow | DI8 | Tool input 0 |
| 5 | Gray | Power | 24V DC |
| 6 | Pink | DO9 | Tool output 1 |
| 7 | Blue | DO8 | Tool output 0 |
| 8 | Red | GND | 0V DC |

**Figure 3.3:** The pinout of the OnRobot RG6 gripper [38].

the pins of interest are pins number 1,3 and 4, more specifically:

- Tool analog input number 2 (AI2)
- Tool digital input number 0 (DI0)
- Tool digital input number 1 (DI1)

these inputs can be used to get the desired feedback from the gripper. The AI2 pin offers a means of an analog feedback and as such, outputs a voltage corresponding to the width of the gripper fingers (This analog sensor proved to be quite noisy and extra measures were taken when plotting the output.). The Polyscope OS can measure said voltage and we can use it as a condition or simply to get the measurement value. The DI0 sets two digital flags, the low state signalizes that the gripper has reached its position and likewise, the high state signalizes that the set force has been reached. Lastly, the DI1 signalizes if the gripper is busy (low state) or ready (high state).Both of these

digital inputs are used as control conditions in the implemented gripping program.

#### Robotiq FT 300 force/torque

The UR10e is also equipped with a Robotiq FT 300 force/torque sensor that has a measuring range $\pm 300\,\mathrm{N}$ and $\pm 30\,\mathrm{N} \cdot \mathrm{m}$ for every axis in Cartesian coordinate system. Another advantage is that the sensor noise is very low $0.033\,\%$ for the force measurements and $0.016\,\%$ for the torque). It comes with special feedback functions for the Polyscope [40].


**Figure 3.4:** The Robotiq FT300 sensor [41].

### 3.1.2 Software

Following control options for the UR10e were explored:

1. UR ROS driver

   From the very beginning of the project the intent was to control the robot and the gripper through Robot Operating System (ROS) as it is very versatile environment, simple to use, quick to implement and commonly used. The Universal Robots have their own regularly maintained and updated Github repository (see [42]) that contains various examples for own URCap development and a ROS driver suitable for our application (see [43]).

   This driver works on both current ROS distributions Kinetic (the older) as well as Melodic (the newest at the time of writing this document). The installation of the driver is described at [43] and consists of the following steps:

   a. cloning the Github repository to a new catkin workspace and building the package,

   b. setting up communication with the UR10e unit by connecting a laptop with the control box of the robot,

   c. installation of the external communication URCap to the teach pendant,

d. the GUI joint controller can be launched to verify the correct functionality. This allows remote operation of the robot, but not of the OnRobot RG6 gripper.

2. The Dashboard server

Next mean of remote control (described at [44]) is the DashBoard server (see [45]). One can utilize the DashBoard server interface for controlling the UR10e Robot from the remote computer by sending simple commands to the robot GUI over a TCP/IP socket. The DashBoard server is running on port 29999 of the robot's IP address. It offers variety of simple commands like turning on/off the robot, loading a program, playing it, etc. Every command must be terminated by a newline.

During the testing phase, the DashBoard server returned correct values to received commands sent to the server using the SocketTest applet [46]. While it works correctly, it is too simple for purposes of this thesis, the only use would be for running the Polyscope programs remotely.

3. The Real-Time Data Exchange (RTDE) interface

The Real-Time Data Exchange (RTDE) interface can be used to synchronize the remote computer with the UR controller again over a TCP/IP socket connection and exchange important information about the robot while maintaining all the real-time properties of the UR controller. The [47] states, that this functionality is mainly useful for interacting with the robot drivers, manipulating robot I/Os and plotting robot status (e.g., robot trajectories).

The RTDE interface is available when the robot is running and it is located on port 30004 of the robots IP address. Using this option requires studying complicated UR RTDE protocol and implementing a custom TCP/IP client, that receives the data and sends back the replies. Therefore, it is beyond the scope of this task.

4. The Polyscope OS and UR scripts

As mentioned above, the gripper comes with its own URCap one can use to control it. The URCap enables the user to utilize control parameters and variables when used as an URScript function. The most important parameters are

- `target_width`
- `target_force`
- `depth_compensation`

The description is in the Table 3.1.

The script function in the Polyscope can be used as follows:

```
RG6(target_width=110, target_force=40, payload=0.0,
set_payload=False, depth_compensation=False, slave=False)
```

| Parameter | Unit | Description |
|---|---|---|
| `target_width` | `[mm]` | Sets width between the gripper fingers |
| `target_force` | `[N]` | Sets force of the gripper |
| `depth_compensation` | `True/False` | Sets on/off the depth compensation |

**Table 3.1:** Description of the OnRobot RG6 function parameters [48].

The feedback variables are

- `grip_detected`
- `lost_grip`
- `measure_width`

They are described in the Table 3.2.

| Feedback variable | Unit | Description |
|---|---|---|
| `grip_detected` | `True/False` | True if Gripper has detected a work piece. |
| `lost_grip` | `True/False` | True if Gripper has dropped a work piece. |
| `measure_width` | `True/False` | Width between the fingers of the gripper. |

**Table 3.2:** Description of the OnRobot RG6 feedback variables [48].

The Robotiq FT 300 sensor can also be controlled from the Polyscope OS [49]. The used functions are

- `get_sensor_Fz()` – function allows the user to assign the force value to a variable;
- `get_sensor_Mz()` – function allows the user to assign the torque value to a variable;
- `get_applied_tcp_force(<index>)` – function returns the current force and torque vector value currently applied at the tool center point.

We can use the parameters and the feedback variables as conditions for our gripping program implementation as described in [48].

We decided to implement our own simple Polyscope program as it offers the best functionality for our case. For a robot-computer communication another program was implemented as described in [50]. The Polyscope and the URScript come with prepared functions for socket communication and so the teach pedant was used as a client and the laptop as a server (as illustrated in the Figure 3.5). The client sends the measurements data to the computer where it can be easily saved into a file.

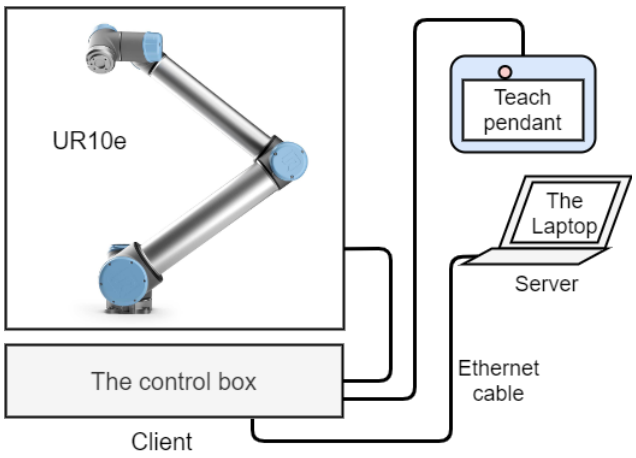


**Figure 3.5:** A connection diagram for the UR10e.

### 3.1.3 The implemented gripping program

The Polyscope OS is a simple and easy to navigate user interface that allows the user to build the program from a wide variety of function blocks. One just uses the desired block and simply builds up a program tree structure one by one. The methods and function descriptions are very well documented in the user manual (see [35]).

For our purposes, mainly the "Script" block was used, that allowed us to use custom URScript code at any part of the program. This way, we could specify the parameters for the OnRobot RG6 gripper script, define new control variables and send the data to the dedicated computer through the socket connection (as the socket script functions are not present as function blocks). The URScript language and all the URScript functions are documented in the URScript manual (see [51]).

The gripping program function is illustrated with the following pseudocode:

```
void grippingProgram {
    target_width = 120;
    target_force = 25;
    open_socket_connection();
    while ( true ) {
        if ( target_width < 25 || target_force > 120 ){
            break;
        }
        //send the command to the gripper
        RG6(target_width, target_force);
        if ( force_reached == true ) {
            //increment the gripping force
            target_force = target_force+1;
        }
        if ( target_width == measure_width ) {
            //decrement the gripper width
```

```
            target_width = target_width-1;
        }
        send_measurements();
    }
    close_socket_connection();
    return;
}
```

The program is sending the measurement data to the remote computer through the socket connection. A Socket test program [46] was used to configure a simple client that can receive the socket messages. The data can then be conveniently saved into a text file. The suitable format ensures simple import to MATLAB. When plotting the data, the relation between the gripping force and the width between the gripper fingers should be observable.

## 3.2 Kinova Gen3 with the Robotiq 2F-85

Next robotic setup is the Kinova Gen3 robot equipped with a Robotiq 2F-85 gripper. The Robotiq 2F-85 gripper can provide various feedback options like motor temperature and voltage. However, the most important for our case proved to be the width between the two fingers and the motor current. Kinova provides a ROS driver for this setup which was used for the control. The robot camera could be also used to record the gripping. For the data acquisition a logging node in C++ was implemented.

### 3.2.1 Hardware

The Kinova Gen3 is a small versatile robot that has 7 DOF and comes with an embedded 2D/3D vision module and a Quick Connect controller. The Kinova support offers well documented manuals, tutorials and sources for ROS packages that allow controlling the robot arm, the gripper and the robot camera. There are also code examples available that can be used for quick understanding of the robot and its functions [52]. The robot is shown in Figure 3.6. The robot comes as standard equipped with a Robotiq 2F-85 adaptive gripper. This gripper has 2 fingers with an 85 mm stroke and offers a grip force from 20 N to 235 N [54]. The gripper is show in Figure 3.7. The fingertips dimensions can be approximated to a rectangle of $37.5 \times 22$ mm. As shown in the Figure 3.8.

### 3.2.2 Software

The Gen3 robot is recommended to be used with ROS and with provided packages (ROS Kortex, ROS Kortex Vision) which proved to be quite useful for our case. The Kortex API documents all the classes and functions that can be utilized while ROS Kortex provides all the sources. The installation process for the ROS kortex and the ROS Vision packages is described in the respective manuals and can be accessed at [57] and [58].

**Figure 3.6:** The Kinova Gen3 robot [53].


**Figure 3.7:** The Robotiq 2F-85 gripper [55].

The process is as follows:

1. clone the packages into a workspace and build it;
2. connect the robot to the computer via the Ethernet cable or the WiFi;
3. launch the Kortex driver with the following command

```
roslaunch kortex_driver kortex_driver.launch ip_address:=
192.168.210.126 start_rviz:=false
```

4. the driver sets up the communication and initializes all the topics and services;
5. an example node or a custom one can be run.

The `/my_gen3/base_feedback` topic was utilized to receive the feedback message. Based on the API the structure of the feedback message is as follows:

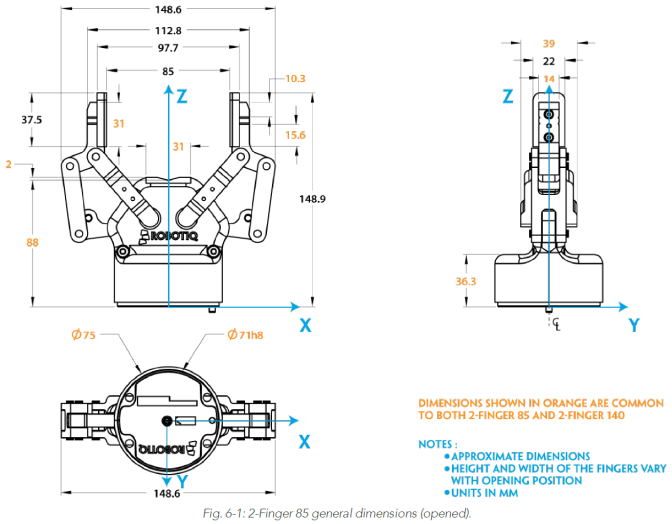


**Figure 3.8:** The Robotiq 2F-85 gripper dimensions [56]

`feedback->interconnect.oneof_tool_feedback.gripper_feedback[0].motor[0]`
The respective classes and parent topics are as follows:

- `feedback` – `BaseCyclic_Feedback`, Parent topic: BaseCyclic (C++)
- `interconnect` – `InterconnectCyclic_Feedback`, Parent topic: InterconnectCyclic (C++)
- `oneof_tool_feedback` – `InterconnectCyclic_Feedback_tool_feedback`
- `gripper_feedback` – `GripperCyclic_Feedback[]`, Parent topic: GripperCyclic (C++)
- `motor` – `MotorFeedback[]`, Parent topic: GripperCyclic (C++)

The camera feed can be accessed by `ros_kortex_vision`. The requirements are identical as for the ROS kortex. This application requires a reliable connection to the robot as the stream needs a high transfer rate. Therefore, mainly the Ethernet connection was used. The process is as follows:

1. launch the kortex driver with a following command
   ```
   roslaunch kortex_driver kortex_driver.launch ip_address:=
   192.168.1.10 start_rviz:=false.
   ```
2. launch the kortex vision node with a command
   ```
   roslaunch kinova_vision kinova_vision_color_only.launch
   ```
3. To observe the stream run the `image_view` with
   ```
   rosrun image_view image_view image:=/camera/color/image_raw
   ```

4. to record the stream run

```
rosrun image_view video_recorder _fps:=30 image:=
/camera/color/image_raw
```

.

### 3.2.3 The implemented gripping program

The gripper has two control modes

1. position control mode,
2. velocity control mode.

Therefore, the position that the gripper is supposed to reach or the closing speed of the gripper can be set. During the experiments the velocity control proved to be more versatile. The closing speed can be set and controlled based on the position of the gripper fingers. A closed loop feedback based on the motor current value can be used as well.

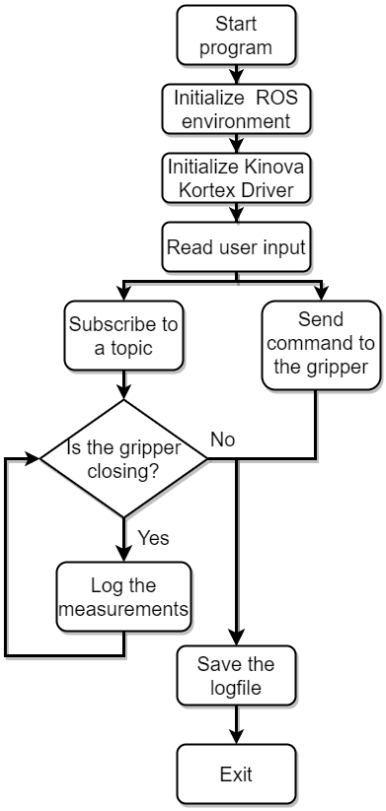


**Figure 3.9:** The Robotiq 2F-85 gripper control program function.

The basic gripper control is explained in the Kinova full arm example. The implementation of the topic subscriber is described in [59]. The gripping program is implemented so the user can set the closing speed, turn on/off the

logging and specify the name of the log file. The command to the gripper is sent by a thread, while a logging loop is running in the second thread. When the gripper is closed, the measured data are saved into a textfile. The implemented control program function is illustrated in the Figure 3.9. The implemented ROS package can be found in the `Kinova_Gen3/kinova_gripping` folder in the Gitlab repository [33].

## 3.3 qbrobotics SoftHand

The next gripper is the SoftHand (Research) by qbrobotics. This device can provide measurements of the motor position which correspond to the fingers position and the current. While it can be mounted on the UR10e robot, it was decided to use it separately, control it via ROS and gather the data with an implemented logging node.

### 3.3.1 Hardware

The qbrobotics describe the SoftHand as an anthropomorphic robotic hand that is flexible, adaptable and able to interact with the surrounding environment. Thanks to its compliance, it limits the risk of hurting the operators or damaging the robot itself [60]. While flexible and highly movable, the qbrobotics SoftHand only uses one electric motor that controls the closing and opening. It can reach a grasp force of 62 N and has a nominal payload of 1.7 kg. The device can thus be utilized for gripping different objects without any change in the program or the device setup. The device is shown in Figure 3.10.

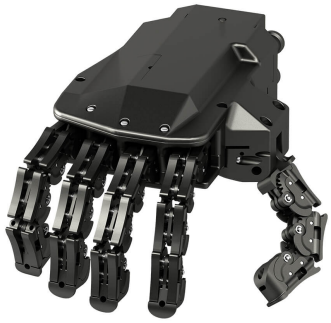

**Figure 3.10:** The qbrobotics SoftHand gripper [61].

The hand can be mounted on the UR10e and controlled via an URCap in the Polyscope OS. However, for a convenience the device was used as a standalone setup that can be connected to the laptop. The available control options described in [62] are as follows:

- through ROS, [63];

- through C/C++ API, [64];
- through MATLAB/Simulink library, [65];

and offer several ways to enable enhanced control modes.

The ROS control was chosen for its simple implementation and proved to be preferable to the other options. The qbrobotics SoftHand manual (see [62]) documents all the options for the remote control of the device. To set up the hand

1. connect the qb control box to the computer via USB,
2. connect the hand and the control box with a corresponding cable,
3. supply a 24 V, 0.6 A DC power to the qb control box.

The picture of the setup is shown in Figure 3.11. The procedure is more specified in the user manual (see [62]).

**Figure 3.11:** The qbrobotics SoftHand standalone setup.

### 3.3.2 Software

The qbrobotics SoftHand ROS packages installation is described in the chapter 6.3 of the software manual (see [62]). It also presents how to run examples. More documentation for the device and the packages can be found at the ROS website [63], and at the qbrobotics bitbucket page [66]. The ROS packages are suitable for ROS Kinetic as well as ROS Melodic. The installation process is as follows:

1. clone the source files into a workspace and build the packages,
2. launch the communication handler with a command `roslaunch qb_device_driver communication_handler.launch`
3. the communication handler detects the qbrobotics SoftHand device and sets up the connection,

4. launch the SoftHand controller.

The qbrobotics SoftHand controller can be launched with the following command

```
roslaunch qb_hand_control control.launch standalone:=false
activate_on_initialization:=true device_id:=1
use_waypoints:=false use_controller_gui:=true
```

The parameters are as follows:

- `standalone:=false` as the communication handler was launched before, `true` otherwise;
- `activate_on_initialization` should be always `true`;
- The `<actual_device_id>` should be always `1`;
- To use the GUI controller `use_controller_gui:=true`;
- To use the waypoints trajectory control `use_waypoints:=true`.

The waypoints are saved in the `<robot_name>_waypoints.yaml` file located in the `<robot_package>_control/config/` folder.
Example:

```
waypoints:
 -
   time: [1.0]
   joint_positions:
     qbhand1: [0.0]
 -
   time: [2.25, 2.75]
   joint_positions:
     qbhand1: [0.8]
```

More detailed description is in [62].

### 3.3.3 The implemented gripping program

There was not a need to implement a program for gripping as such, instead the GUI control mode was utilized. This way the closing speed and the motor position can be simply set. However, custom ROS node for the measurements logging and then saving it into a text file was implemented. The feedback service is named `GetMeasurements` and it is used for getting the motor position and the motor current. The ROS node periodically calls the service and the results are saved into a text file with an appropriate name and format. The service client implementation is documented in [67]. The ROS package that contains the node for the logging was uploaded to the Gitlab repository at [33] and can be found in the `qb_SoftHand/qbhand_logging folder`.

## 3.4 Festo DHEF gripper

As a comparison to the standard grippers the Festo adaptive shape gripper (shown in Figure 3.12) and its performance was also tested.

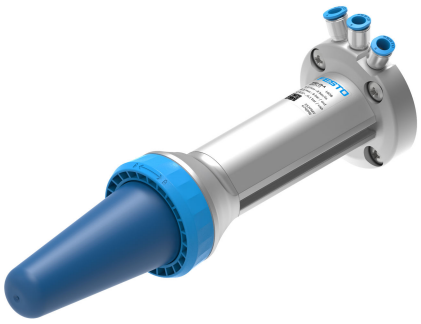

**Figure 3.12:** The Festo DHEF gripper [68].

This manipulator is composed of a pneumatic piston and the inverting rubber cap. The piston is situated inside the gripper and its rod is connected to the inner tip of the cap. When negative pressure is applied to the piston, the rod moves the rubber cap inwards, at this moment any object positioned at the tip from the outside is "sucked" into the cavity made by the motion. The object is held by the constricted rubber cap around it [69].

Festo advertises the manipulator as the best suited for handling small parts, applicable for robot-human workplaces, for pick and place processes where precision and speed are not the priority. According to Festo, the gripper can be equipped with two sensors that measure the piston position and provide feedback. However, this individual gripper did not have these installed, which made the feedback very limited [69].

The testing was very short, manipulation of basic objects was attempted manually and the results were not very impressive. The gripper only has two states depending on the position of the inner piston, they can be described as open and closed. Thus, there is no control between the states and no way how to get the information about the grasped object. Moreover, this manipulator is mostly designed for small rigid objects with hard edges like blocks, bolts and nuts. The gripper had problems picking up bigger flat objects. Therefore, it was decided not to use this particular gripper in this research as it is not suitable for my case. However, it is a very interesting design nonetheless and can be very effective for specific setups.

## 3.5 Physics of deformation

When applying a force on the object formed from an isotropic material the elementary Hook's law in mathematical form can be expressed as

$$\epsilon_{11} = \frac{1}{E}\sigma_{11}, \tag{3.1}$$

where $\sigma_{11}$ is the axial stress and $\epsilon_{11}$ is the axial strain. The subscripts refer to the $x_1$ axis, in other words the strain vector has the same direction as the normal vector. Noting the fact that $\sigma_{11} = \frac{F}{S}$, we can rewrite (3.1) as

$$\epsilon_{11} = \frac{1}{E}\frac{F}{S} = \frac{a' - a}{a} = \frac{\Delta a}{a} \tag{3.2}$$

where $F$ is the applied force to the $x_1$ axis on the cross-sectional area $S$, $a$ is the length before the force was applied, $a'$ is the length afterwards and

$$E = \frac{\sigma_{11}}{\epsilon_{11}} = \frac{F}{S}\frac{a}{a' - a} = \frac{F}{S}\frac{a}{\Delta a} \tag{3.3}$$

is the Young modulus. It shows a relation between the force per unit area and proportional deformation. The deformation can be either tensile or, as in our case, compressive. Young modulus describes the stiffness of the measured object (as used in [12] and [14]).

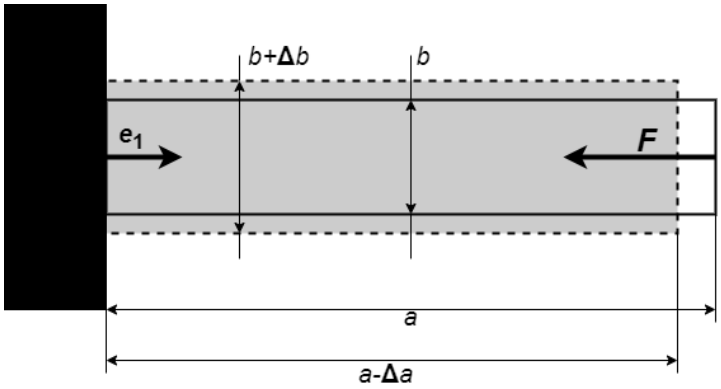


**Figure 3.13:** An illustration of the deformation of a material affected by an applied force. Solid line represent the state before the deformation, dashed line the state after. Adopted from [70].

Another important material property is the ratio of transverse and axial strain. It is called Poisson's constant and can be written as

$$\nu = \left|\frac{\epsilon_{22}}{\epsilon_{11}}\right|. \tag{3.4}$$

The material is being stretched, the axial strain $\epsilon_{11}$ is positive (refers to elongation) and the transverse strain is negative (refers to contraction). If we compress the material, the effect is opposite. The axial strain $\epsilon_{11}$ is

negative (refers to compression) and the transverse strain is positive (refers to expansion). The effect of compressing a material is illustrated in the Figure 3.13, it is clear that the material is compressed in axial direction by $\Delta a$ and thus expanded in transverse direction by $\Delta b$.

Based on Equation 3.4 we can write the Hooke's law for transverse contraction as

$$\epsilon_{22} = -\nu\epsilon_{11} \tag{3.5}$$

or in other form

$$\frac{\Delta b}{b} = -\nu\frac{\Delta a}{a}. \tag{3.6}$$

The Equation 3.6 can be modified for transverse expansion as well [70].

Properties of the grasped objects were determined by using the equation (3.3). The gathered data were modified into a relation of stress and strain (see Section 4.3.2). Since the manufacturer specified the compression stress value at 40 % in the data sheet, the same strain was also selected as a point of interest. The Hooke's law is valid only for a small deformations and materials that exhibit a linear behaviour when deformed. Thus, a linear function was fitted to a close neighbourhood($\pm 5$ %) of the chosen point (see Figure 3.14 and 3.15, for an illustration). The modulus obtained with this method is only valid for that close neighbourhood [71]. However, for some of the objects in some of the setups (mostly for the FT 300 force/torque sensor, and for the cubes and dice set) this was not ideal, so another linear area was located and examined. For the explored materials an extension test would be more appropriate, but not possible to do with the used experimental setup.

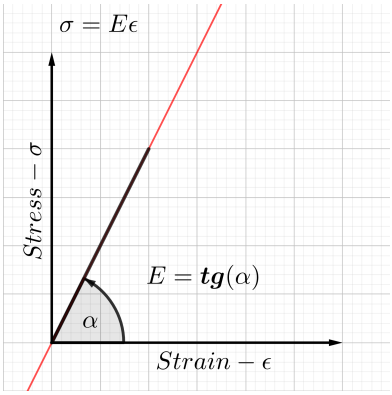


**Figure 3.14:** An illustration of the stress/strain relation and how it is related to Young modulus. Adopted from [71].

The equation (3.3) can be further modified as:

$$E = \frac{\Delta\sigma}{\Delta\epsilon} = \frac{\sigma_2 - \sigma_1}{\epsilon_2 - \epsilon_1} = \frac{\frac{F_2 - F_1}{S}}{\frac{a_2 - a_1}{a_0}} = \left(\frac{\Delta F}{\Delta a}\right)\frac{a_0}{S} \tag{3.7}$$

We can use the equation (3.7) and any two different points from the linear function to get the Young modulus. In other words, the slope of the linear function corresponds to the Young modulus of the material. The same

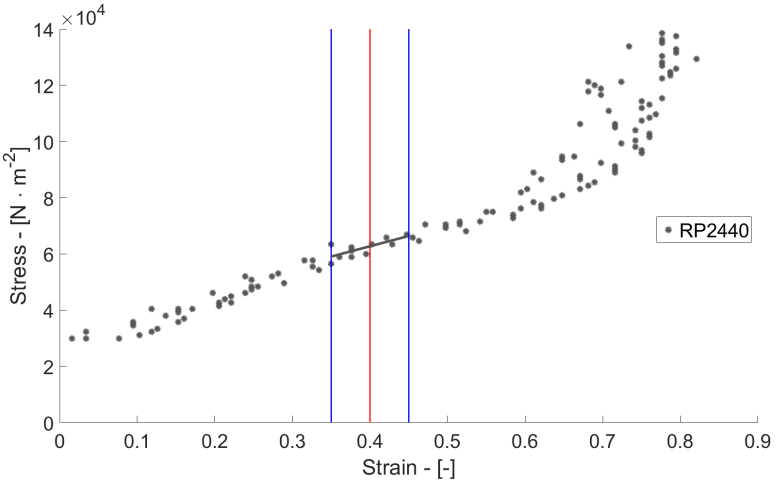


**Figure 3.15:** An example of the linear fit at the point of interest.

approach was used in [72], where a compressive Young moduli of plant stems were measured. Moreover, a research had been conducted with a similar type of material (polyurethane foams used for furniture) and a similar experimental setup (compressing an object with a measuring machine). Smardzewski et al. [73] state that the *polyurethane foams* (not unlike the ones used in this research, see Section 4.1.2) *are characterised by the changing value of the Young modulus at different stages of compression*, which is something that must be taken into account. The relations (again, similar curves to our results, see Section 4.3.2) are shown in Figure 3.16 and the measured moduli are presented in Table 3.3 for a comparison. Typical values for other plastic compounds are shown in the Table 3.4 together with harder materials and can be for a comparison as well.

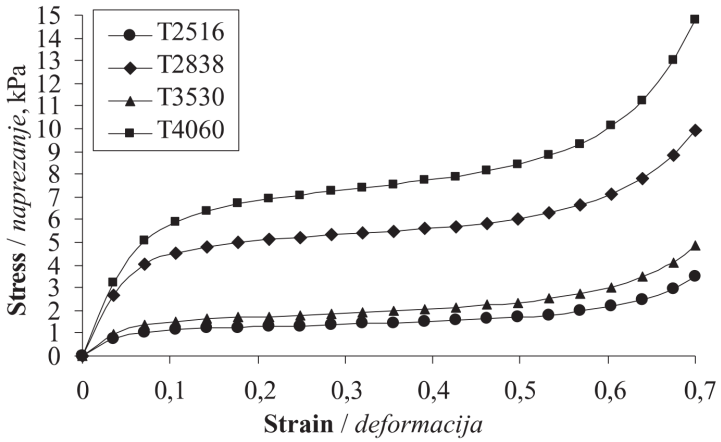


**Figure 3.16:** Relations of polyurethane foams (featured in Table 3.3) in the stress/strain system. Adopted from [73].

| Type of foam | $E_1$ – [GPa] | $E_2$ – [GPa] | $E_3$ – [GPa] |
|---|---|---|---|
| T2516 | 14,44 | 1,52 | 11,06 |
| T2838 | 56,12 | 3,75 | 24,30 |
| T3530 | 18,69 | 2,32 | 15,50 |
| T4060 | 70,25 | 6,22 | 40,82 |

**Table 3.3:** Experimentally gained Young moduli of the polyurethane foams (Notice the similar material names). Sourced from [73].

| Material | Young modulus – [GPa] |
|---|---|
| Rubber, small strain | 0.01 – 0.1 |
| Polyethylene, LDPE (low density) | 0.11 – 0.45 |
| ABS plastics | 1.4 – 3.1 |
| Polypropylene, PP | 1.5 – 2 |
| Chlorinated PVC (CPVC) | 2.9 |
| Epoxy resins | 2 – 3 |
| Acrylic | 3.2 |
| Polystyrene, PS | 3 – 3.5 |
| Silver | 72 |
| Gold | 74 |
| Bronze | 96 – 120 |

**Table 3.4:** Examples of the Young moduli for different materials. Sourced from [74].

## 3.6 Matlab functions

To process the large amount of measured data supportive functions in MATLAB had to be implemented. The raw data were saved in a simple text file. Variables were saved on a single line one after another. Each line represents a single discrete step.

Example:

```
//index measure_width grip_force
1 118.3 20
2 117.6 20
3 119.1 20
...
```

The name of the text file is also important as it contains the name of the gripper, time and date of the measurement, the measured object, the speed of the gripper and other details.

Example:

```
2F85-2020-04-03-17-05-T1820-50-05.txt
```

The textfiles were saved in the dedicated folder for further processing in MATLAB. An implemented MATLAB function `readTxtData` that reads

and loads the data then reads the file name and saves the properties into the measurement structure. A database of MATLAB structures, that contains information about measured objects was also created. The loading function can simply search the database for the unique object ID and then includes the object structure in the measurement structure. The object structure contains information about the object: e.g., compression stress values, dimensions, typo of material, etc. The `readTxtData` connects the measured object id with the object id in the database and assigns the object information to the structure of measured data as well. The data structure thus contains among the measured data also the important information about the particular measurement. For an illustration the functionality schematic is outlined in the Figure 3.17.

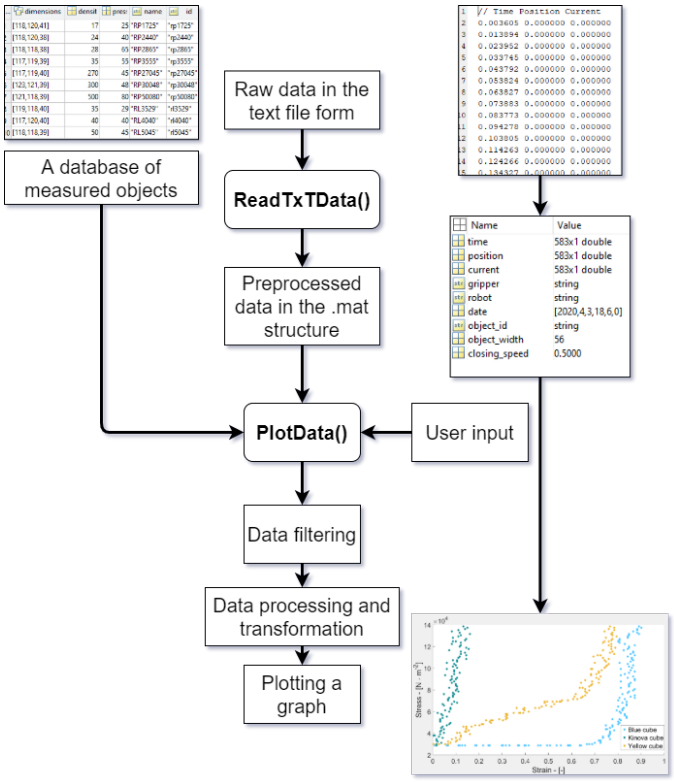


**Figure 3.17:** Schematic of the MATLAB functions.

The data structures are then loaded into the `plotData` function. The measured data are filtered based on the user input, transformed into a relation of stress and strain and finally plotted. The user can decide on the plotting options. It is possible to select the gripper results to be plotted, which objects to show and how to group them. This enables users not familiar with the research to explore the results. The whole platform is simple to understand, use and, if needed, expand. For the computation of the Young moduli and plotting the relation the `plotYoung` script was implemented. The code is uploaded to the Gitlab directory [33] to the `MATLAB_functions` folder, documentation included.

# Chapter 4

# Experiments and results

In this chapter the extension of the YCB dataset by deformable objects is described, the experiments are illustrated, the results presented and interpreted.

## 4.1 Used Objects

To be able to test and evaluate material properties of various objects by various grippers, we needed to create a set of experimental objects. This set should afterwards serve as an extension of the standard YCB dataset (see [8]) as it does not contain a lot of soft homogeneous objects. To remedy this, the extension of this dataset is proposed. This extension should be replicable so that other researchers can create experiments on this extended dataset. Therefore, the intention was to find similarly shaped objects with different stiffness and ideally from a homogeneous material. The emphasis has been put on the everyday nature of the chosen objects—preferably simple household objects that are cheap and available to everyone. The worldwide availability was considered, so the other members of the IPALM consortium could obtain the objects and extend their datasets.

The initial pilot set was formed from various kitchen sponges, children toys and similar objects. This set is more described in Section 4.1.1 (*Pilot set*) and the results are presented in Section 4.3.1.

After we tested the pilot set and examined the results, we searched for more suitable objects. The mechanical response of an object is a result of the combination of object material and shape. Therefore, as our main interest is stiffness/elasticity, it was decided to choose objects with simple shapes and uniform material composition. The priority were block shaped objects of different materials, as the force-compression relation is strongly dependant on shape. Thus, ball shaped or even more complicated objects are difficult to examine properly. To approach this, a set of cubes of different sizes, materials and therefore also stiffness was created. To tackle the variable size and shape, the same sized cubes were cut out of different materials. This set is described in Section 4.1.3 (*Cube set*) and the results for this set are presented in Section 4.3.2.

Last but not least, a set of twenty different polyurethane objects of similar

shapes was obtained. These materials comply with the ISO standards and come with a technical data sheet to reference the material properties. The set is presented in Section 4.1.2 (*Polyurethane foams set*) and the results are in Section 4.3.2.

### 4.1.1 Pilot object set

The initial object set contains 13 objects (shown in Figure 4.1). The set contains various sponges for various purposes. These sponges are made from varying materials, have different textures and elasticity. The rest are multiple cubes/blocks and some toys. The chosen objects are mainly very soft and homogeneous, the exceptions are the green wooden block, which represents a solid object, the kitchen dish sponge, that is formed out of two materials and the washing sponge that is wrapped in leather or plastic. Some suitable objects from the YCB dataset were also tested.

The lack of homogeneity can bias the measurements. The same can be said about the objects with complicated shapes. For example, it is difficult to decide how to orientate the bath duck in the gripper. The shape of the object does affect the measurement. Another disadvantage is the scarceness of information about the materials. The rest of the tested objects were excluded from this set for being too stiff for some of the grippers.

**Figure 4.1:** Pilot set of objects.

### 4.1.2 Polyurethane foams set

We managed to obtain a set of 20 different polyurethane samples (shown in the Figure 4.2) directly from a distributor ([75]). These samples are roughly of the same size and shape, ideal for grasping. The foams each have specific purpose. The set includes hard insulation foams, memory foams, mattress foams and soundproof foams. Each sample has a different apparent core density and compression stress value.

The characteristics of each sample were specified by the distributor and data sheets. Therefore, this information can be used as a reference and


**Figure 4.2:** Polyurethane foams set of objects.

compared with the measurements. An example of the information given by the manufacturer is shown in Table 4.1. The materials comply with several ISO standards: e.g., EN ISO 845, EN ISO 3386, EN ISO 2439 and EN ISO 1798. The materials were grouped according to the material type. The dimensions of the materials, ordered from the lowest compression stress value to highest, are shown in Table 4.2. Notice that the last two numbers in the material name represent the compression stress value at 40 % of the material. E.g., the RP2440 material has the compression stress value value at 40 % of 4.0 kPa. For the reader's convenience this number is highlighted in bold throughout this chapter. The advantage of this set is that in case of necessity a large quantity of said materials can be ordered with constant quality and a large variety of objects can be manufactured for measuring purposes.

| **Attribute Name** | **RP2440** | **RP30048** | **ISO standard** |
|---|---|---|---|
| Quality | RP24**40** | RP300**48** | |
| Material | Richfoam Polyether | Richfoam Polyether | |
| Standard colour | white | white/lightblue | |
| $\rho_a$ – [kg/m$^3$][1] | 20.9 – 23.1 | 26.6 – 29.4 | EN ISO 845 |
| $CV_{40}$[2]– [kPa] | 3.4 – 4.6 | 4.1 – 5.5 | EN ISO 3386 |
| Indentation hardness[3]– [N] | 127 – 173 | 170 – 230 | EN ISO 2439 |
| TS[4]– [kPa] | > 90 | > 130 | EN ISO 1798 |
| $E_b$[5]– [%] | > 130 | > 150 | EN ISO 1798 |

**Table 4.1:** Example of the information from the technical data sheet. Sourced from [76].

[1] Apparent core density
[2] Compression stress value at 40 %
[3] at 40 % compression
[4] Tensile strength
[5] Elongation at break

| Type | Dimensions – [mm] |
|---|---|
| **RP type** | |
| RP17**25** | 118 × 120 × 41 |
| RP24**40** | 118 × 120 × 38 |
| RP27**045** | 117 × 119 × 39 |
| RP30**048** | 123 × 121 × 39 |
| RP35**55** | 117 × 119 × 39 |
| RP28**65** | 118 × 118 × 38 |
| RP500**80** | 121 × 118 × 39 |
| **RL and N type** | |
| RL35**29** | 119 × 118 × 40 |
| NF21**40** | 105 × 100 × 50 |
| RL40**40** | 117 × 120 × 40 |
| RL50**45** | 118 × 118 × 39 |
| N40**72** | 118 × 117 × 37 |
| **T type** | |
| T18**20** | 125 × 125 × 50 |
| T20**30** | 125 × 120 × 40 |
| T32**40** | 123 × 123 × 50 |
| T25**45** | 125 × 125 × 50 |
| **V and GV type** | |
| V45**15** | 118 × 120 × 40 |
| V50**15** | 119 × 120 × 42 |
| GV50**30** | 118 × 119 × 40 |
| GV50**40** | 118 × 118 × 39 |

**Table 4.2:** Polyurethane foams set dimensions. The materials are listed based on the compression stress values (in bold) obtained from the manufacturer.

### 4.1.3 Cubes and dice set

As a final set, 7 cubes were gathered. For our purposes, the cube as a rectangular object proved to be the best shape as its sides are orthogonal to the applied gripping force and in case of homogeneous material the orientation of the sides can be ignored. The set can be divided into 3 cubes and 4 dice (shown in Figure 4.4).

The promo cube from Kinova proved to have ideal dimensions and so the same shaped cubes were cut out of the yellow sponge and a big blue die. This way 3 cubes of the same shape and size can be compared, but their material varies. The 4 dice (all ordered from Amazon) are the same shape, different sizes and different materials.

All the objects in the set are unified in terms of shape/geometry, the cubes can be reproduced, others can be obtained worldwide. The cube shape proved to be simple to grasp and compress as the gripper jaws are level with the surface. The gripping force is then applied perpendicularly to the object surface as illustrated in the Figure 4.3. The dimensions of the objects are

shown in the Table 4.3.

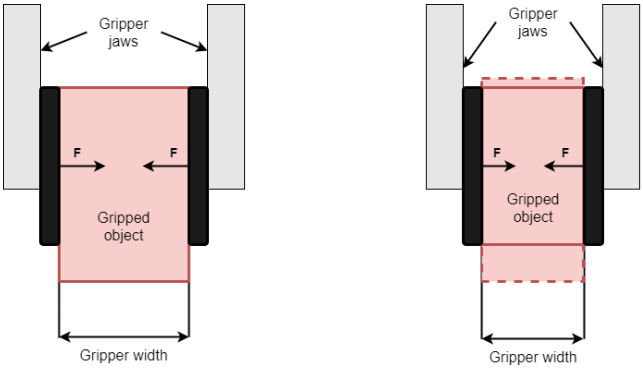


**(a) :** Before the gripping.

**(b) :** After the gripping.

**Figure 4.3:** Illustration of the gripping process for the OnRobot RG6 and Robotiq 2F-85 grippers.

| Object name | Dimensions – [mm] |
|---|---|
| **Cubes** | |
| Kinova cube | $56 \times 56 \times 56$ |
| Blue cube | $56 \times 56 \times 56$ |
| Yellow cube | $56 \times 56 \times 56$ |
| **Dice** | |
| Darkblue die | $43 \times 43 \times 43$ |
| White die | $59 \times 59 \times 59$ |
| Pink die | $75 \times 75 \times 75$ |
| Blue die | $90 \times 90 \times 90$ |

**Table 4.3:** Cubes and dice set dimensions.

## 4.2 The object gripping

The robotic setups described in Chapter 3, provide a wide range of possibilities how to execute the measured gripping.

Depending on the gripper, we varied:

- gripper jaws;
- closing speeds;
- orientations;
- closing and opening multiple times.

Some of the gripping and squeezing sessions were recorded using a Sony video camera and two Intel RealSense cameras to allow for subsequent


**Figure 4.4:** Set of cubes.

analysis—not performed here. Selected recordings were uploaded to the Google Drive directory at [77] and are located in the `Videos` folder. The individual gripping processes for each gripper are described in its respective subsections.

### 4.2.1 OnRobot RG6

**Gripping process**: As the OnRobot RG6 offers the most basic control (see Section 3.1.1), the gripping process was the simplest out of the three. The gripper was slowly closing step-wise while increasing the force when necessary. This way, only one closing speed setting was used and it is important to emphasize that the closing movement itself was not continuous. Basically, the gripper gradually decremented the position between its jaws with a certain force. When the position could not be reached, the force was incremented. This way a relation of reached force and position can be explored. The gripping of the objects is illustrated in Figure 4.5a. For more detailed description of the implemented gripping program, see Section 3.1.2 and 3.1.3.

**Pilot set**: Firstly, we tested the objects that were afterwards grouped into the pilot set (see Section 4.1.1). We ruled out the objects that were too stiff to compress for the qbrobotics SoftHand and even for the OnRobot RG6 gripper as they have small reachable force (62 and 120 N respectively). We were trying different orientations and settings to determine the best approach. Moreover, the Airskin had to be removed around the gripper as it was interfering with the grasped objects.

**PU foam set**: Then we tested all the objects out of the polyurethane foams set (see Section 4.1.2) multiple times. We were gripping the object in the middle so the gripper jaws would be level with the surface. The gripper was oriented from the top, facing down, and its jaws were parallel with the grasped object as illustrated in Figure 4.5a. The object width and the surface area of the gripper jaws is known. Therefore, the gripper width (gripper jaws span) can be transformed into object compression and then into strain (the object compression is divided by the object width). The pressure (stress)

value was computed from the gripping force (see Equation 3.7 in Section 3.5 for more detail). The surface area of the jaws was considered as a cross-section area included in the modulus calculation.

**Cube set**: Finally, with the same approach the cube set (see Section 4.1.3) was tested.

**(a) :** OnRobot RG6 gripper gripping a foam object.

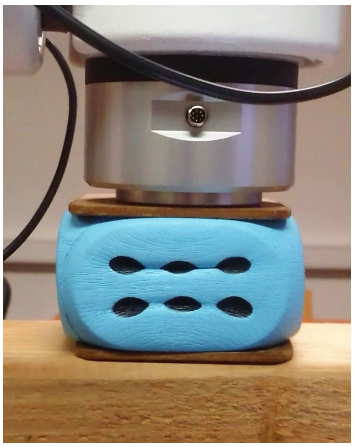

**(b) :** FT300 squeezing a blue die.

**Figure 4.5:** An Illustration of the OnRobot RG6 gripper and Robotiq FT 300 force/torque sensor.

### 4.2.2 Robotiq FT 300

The very precise force/torque sensor Robotiq FT 300 mounted on the UR10e (see Section 3.1.1) is ideal for comparison purposes. It was used to measure the properties of the cube set and the foam set and the results was compared with the measurements from the other grippers.

The measured force and torque can be conveniently related to the object compression. The force was measured in the z axis only. The object size is known, but since the sensor is quite precise, the moment of touch is clearly apparent from the plots. The software options are described in Section 3.1.2.

**Gripping process**: Special pads ($95 \times 95\,\text{mm}$) for a better area coverage were used and one speed setting only. The sensor was moving perpendicularly (only in the z axis) to the top side of the object with the speed of $30\,\text{mm} \cdot \text{s}^{-1}$ and pressing it in between two said pads (see Figure 4.5b, for an illustration). When a force of 90 N was reached (limitation of the UR10e robotic arm), the sensor was moved back to the starting position with the speed of $60\,\text{mm} \cdot \text{s}^{-1}$. As the pads are larger than the side area of the objects, the object surface area of the top (and bottom) side was used as a cross-section area for the pressure (stress) value computation. The relation of stress and object compression can be then transformed into a relation of stress and strain and thus the Young modulus can be computed as well (see Equation 3.7 in Section 3.5 for more detail).

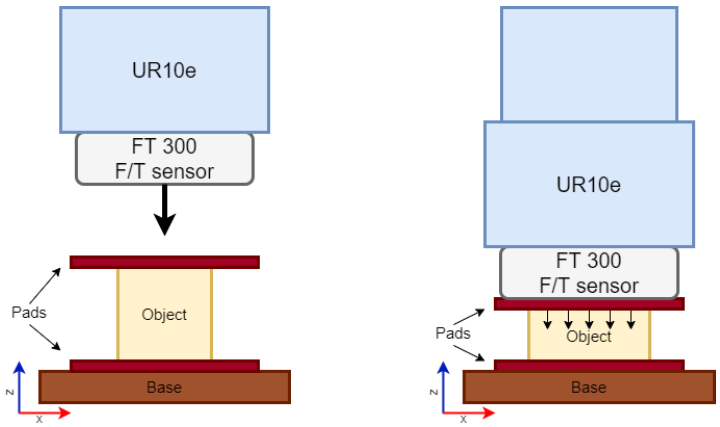


**(a) :** Before the descend. **(b) :** After the descend.

**Figure 4.6:** Illustration of the squeezing process for the Robotiq FT 300 force/-torque sensor.

**Testing sets**: These results can be used for additional comparison to the grippers. In Figures 4.18d to 4.21d of polyurethane objects measurements the hysteresis can be seen as the squeezing and release was measured. For the cubes and dice in Figure 4.23d only the squeezing was measured.

### 4.2.3 Robotiq 2F-85 gripper

Next, the Robotiq 2F-85 gripper offers the best amount of control out of the three grippers (see Section 3.2). It is also the strongest gripper (it can reach a force of 235 N, [54]) and based on the prior measurements, it seems to be the most sensitive one as well (with the exception of the Robotiq FT 300 force/torque sensor). The logging program was set with a logging rate of 100 Hz, but it is apparent from the measurements that the refresh rate of the gripper sensors is several times slower.

The most important output proved to be the gripper jaws span and the gripper motor current. As the object width is known, the jaws span can be transformed into object compression and then into strain (similary as in Section 4.2.1). However, the second gripper output is current (A) rather than force (N). Therefore, an assumption was made that the current is analogous to the gripping force, as the relation of current and strain was very similar to the relation of force and strain of other grippers. More information about the implemented gripping program is provided in Section 3.2.3.

**Gripping process**: A similar approach as in the case of the OnRobot RG6 (see Section 4.2.1) was used. The gripper was positioned so the jaws compressed the object in its half, parallel and flush with the surface (see Figure 4.7). The gripper was oriented from the top, facing down, as in the preceding case.

**Testing sets**: As the Robotiq 2F-85 turned out to be the most user friendly to operate, it was utilized the most. The pilot set was used for the initial testing and then the focus gradually moved to the cube and foams sets.

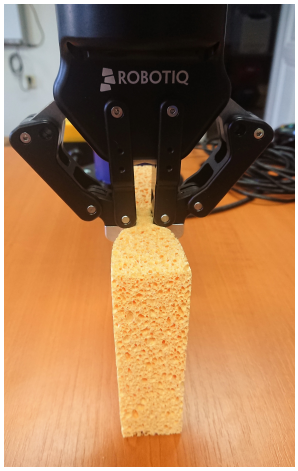


**Figure 4.7:** Robotiq 2F-85 gripper grasping a sponge.

Unlike the OnRobot RG6 gripper, gripping the object with various speeds (from very slow to the fastest possible) could be explored. According to the data sheet the gripping speeds can be 20 to 150 $\mathrm{mm} \cdot \mathrm{s}^{-1}$ [56]. The results of the experimental closing of the empty gripper are in the Table 4.4. The best closing speed transpired to be the 50 % setting. Example of measurements with different closing speeds is in the Figure 4.24. However, the listed speeds are only nominal ones of the empty gripper as the closing speed reduced when the jaws got in contact with the grasped object. The closing was thus not constant for the whole duration of the grasping, as the gripper is not powerful enough, but it is a sufficient approximation.

| **Gripper speed setting** | **Real closing speed -** $[\mathrm{mm} \cdot \mathrm{s}^{-1}]$ |
|---|---|
| 30 % | 54.87 |
| 50 % | 79.10 |
| 80 % | 108.96 |
| 100 % | 131.33 |

**Table 4.4:** Experimentally gained closing speeds.

A gripping routine where the gripper grasps and releases the object multiple times was also implemented. This way a change in resistance due to the material memory might be observable—not presented in this work.

### 4.2.4 qbrobotics SoftHand

Same as the Robotiq 2F-85 gripper, the qbrobotics SoftHand offers a speed control mode (see Section 3.3.2 and 3.3.3), so how different closing speeds affect the measurements could be explored.

**Gripping process**: The issue that emerged was where to position the object to guarantee a stable grip. Naturally, the design of the qbrobotics SoftHand is sensitive to the shape of the objects. Mainly the position of the

thumb and its movement proved to be counterproductive to the measuring process as it was sometimes pushing against other fingers. Due to the cable control the hand does not close exactly the same for every closing process. This brings undesirable variance to the measurement. An emphasis was put on positioning and orienting the objects identically on the palm of the hand. The object was situated so the fingertips, when closed, were parallel with the object surface and the gripping force was applied perpendicularly to the top side of the object (see Figure 4.8a).

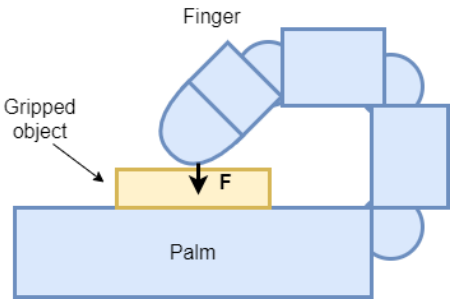


**(a) :** Schematics of the qbrobotics SoftHand gripping an object.

**(b) :** qbrobotics SoftHand grasping a wooden block.

**Figure 4.8:** Illustration of the qbrobotics SoftHand gripping an object and an example.

However, this proved to be quite difficult to achieve, as it can be seen in the Figure 4.8b. It is apparent in the figure that not all the fingers are gripping the cube properly. However, when all the fingers are gripping the object the results are more stable.

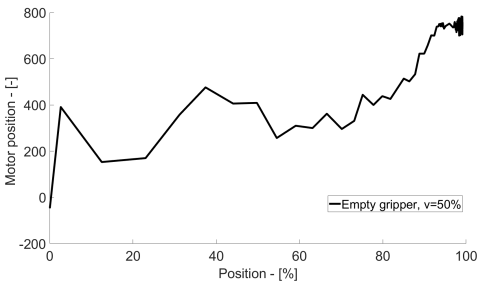


**(a) :** Relation of the motor current on the gripper position.

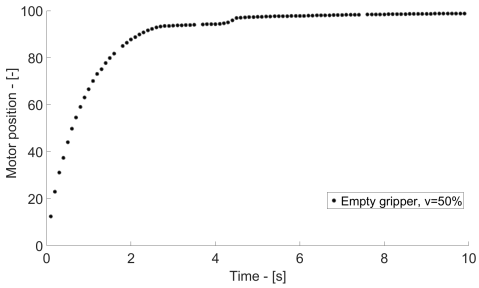


**(b) :** Relation of the gripper position on time.

**Figure 4.9:** Comparison of closing the empty qbrobotics SoftHand.

**Empty gripper**: For a comparison, the measurements for an empty gripper were plotted. The graphs are shown in Figure 4.9. Based on the early measurements of the pilot set, only the phase of grasping between 60 % to 90 % of closure seems to be useful. The output data are representing a relation of the motor current and the motor encoder output, which can be

transformed into percentages of closure. The result is very cluttered and not very informative, as can be seen in Figure 4.10. The data are also very noisy and the measurement of an empty gripper is not very different from the object gripping. For this reason, the reached position of the gripper after a certain amount of time seems to be more informative and it was thus chosen for the results representation.

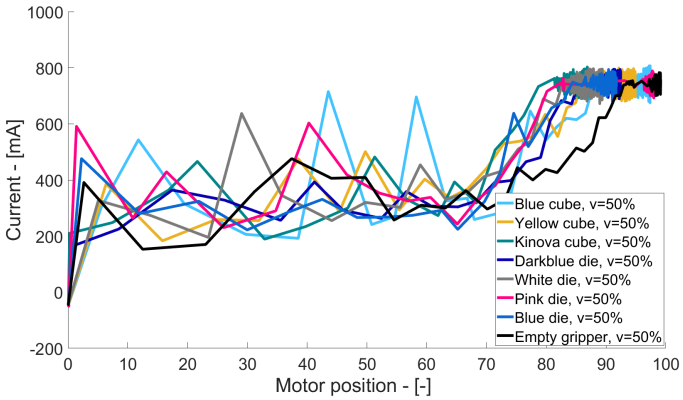


**Figure 4.10:** A relation of the motor current on the position of the qbrobotics SoftHand gripper on the cube and dice set.

**Testing sets**: After the testing of the pilot dataset with various speeds (10 %, 50 % and 100 %) it became clear that the object shape and geometry must be unified. This was done by using the same shape (cube) with similar dimensions. Thus, the polyurethane foams set and the cube set were had been tested multiple times.

## 4.3 Results

In this section, selected results are presented and interpreted. The results for each object set and material type (in case of the polyurethane foams) are situated in its respective subsection. The computed Young moduli (see Section 3.5, Equation 3.7) are also included. The resulting relations were also uploaded to the Google Drive directory at [77] and are located in the `Results` folder.

To select the proper format of the graphs, comparisons of two types of outputs (MATLAB functions `scatter` and `plot`) are provided and the more suitable one for every gripper is chosen. For the OnRobot RG6 gripper graphs, based on the comparison of relations in Figure 4.11a, and 4.11b, the function `scatter` was chosen to plot the data, as the density of datapoints is sufficiently high. The `plot` function, on the other hand, amplifies the effect on noise present in measuring the gripper instantaneous aperture (see Section 3.1.1).

For the Robotiq 2F-85 gripper the `plot` function was used as the `scatter` is not very clear—the density of datapoints is too low—as shown in Figure 4.12a, and 4.12b.

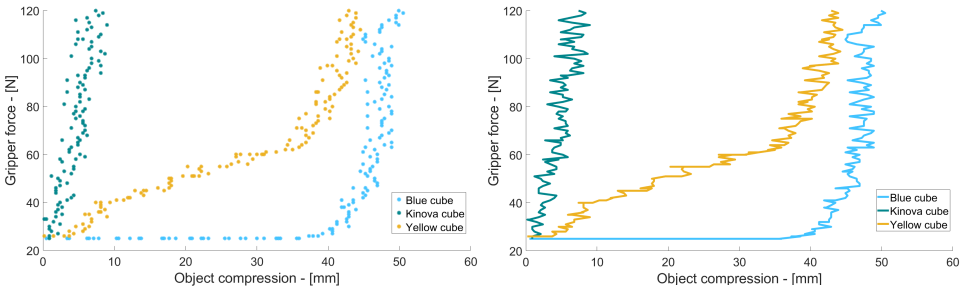


**(a) :** An example of the `scatter` function. **(b) :** An example of the `plot` function.

**Figure 4.11:** Comparison of `plot` and `scatter` for the OnRobot RG6 gripper on the cube set.

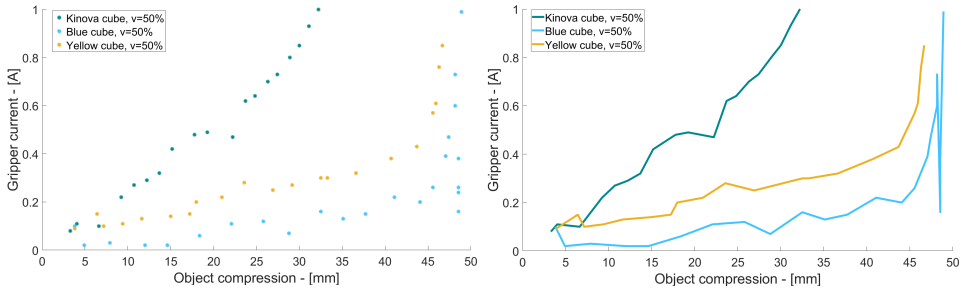


**(a) :** An example of the `scatter` function. **(b) :** An example of the `plot` function.

**Figure 4.12:** Comparison of `plot` and `scatter` for the Robotiq 2F-85 gripper on the cube set.

In the case of the qbrobotics SoftHand the relation of time and position is shown, as the relation of position and current is not very informative (see Figure 4.10 for comparison in Section 4.2.4). This way, the position after a fixed interval can be a good estimation of the material elasticity: for softer materials, the hand closes more, which is visible on the motor position axis. Based on the comparison of relations in Figure 4.13a, and 4.13b, the `scatter` function was used for the results demonstration.

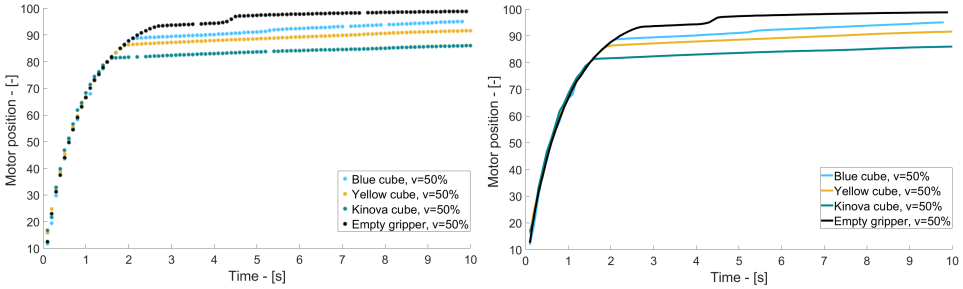


**(a) :** An example of the `scatter` function. **(b) :** An example of the `plot` function.

**Figure 4.13:** Comparison of `plot` and `scatter` for the qbrobotics SoftHand gripper on the cube set.

Based on the comparison of Figure 4.14a, and 4.14b, the `plot` function

was used for the results demonstration for the force/torque sensor Robotiq FT 300. Similarly to Robotiq 2F-85, datapoints are too sparse for `scatter` to give a good overview.

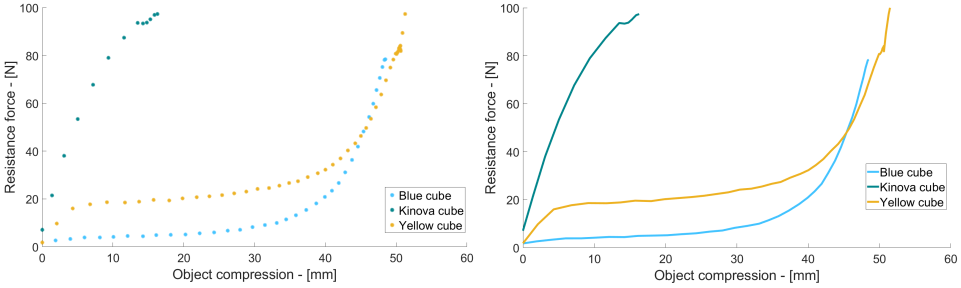


**(a) :** An example of the `scatter` function. **(b) :** An example of the `plot` function.

**Figure 4.14:** Comparison of `plot` and `scatter` for the Robotiq FT 300 force/-torque sensor on the cube set.

### 4.3.1 Pilot set

The Figure 4.15b shows the results of one of the early measurements on the pilot dataset (shown in Figure 4.15a) with the OnRobot RG6 gripper. The effect of different stiffness is clearly observable. The wooden block being a solid object shows no compression at all, while the force rises. On the other hand, the kitchen sponge is distinguished as the softest. In this case, two orientations were measured. The sponge was oriented vertically (width of 39 mm) and horizontally (width of 110 mm). Both relations appear to be exponential, it is more clear for the horizontally oriented sponge. For both cases the final compression is around 77 % of the original width. The stress ball and Kinova cube show more of a linear relation, as they are made out of rubber-like material that is not very porous.

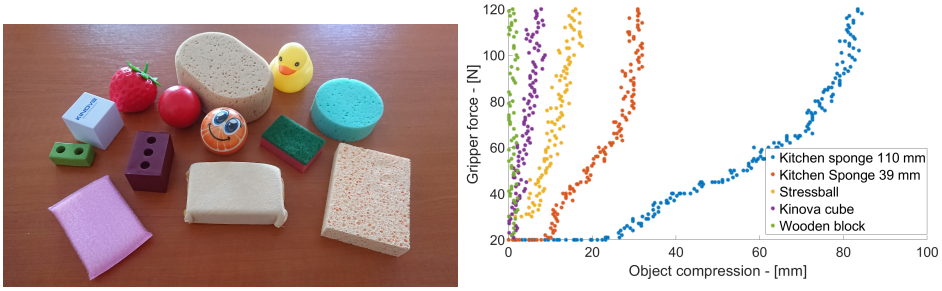


**(a) :** The pilot set of objects.

**(b) :** OnRobot RG6 gripper: Initial test on objects from the pilot set.

**Figure 4.15:** The illustration of the pilot set and the results of the initial gripping test with the OnRobot RG6 gripper.

The Figure 4.17, shows the results of gripping various sponges (see Figure 4.16) from the pilot set with the Robotiq 2F-85 gripper. Each object was measured with 4 different closing speeds. The final compression is very similar

for every speed setting, only the slope of the plotline varies. For some of the lower speed settings, the gripper was not able to sustain the continuous closing until the final compression was reached. This resulted in the oscillations of the current at the end of the plotline. The data of the affected plots were cropped at the end to rectify this.

**Figure 4.16:** Set of sponges, containing (from left to right): sponge 70 mm, sponge 35 mm, car sponge 41 mm, kitchen sponge 40 mm

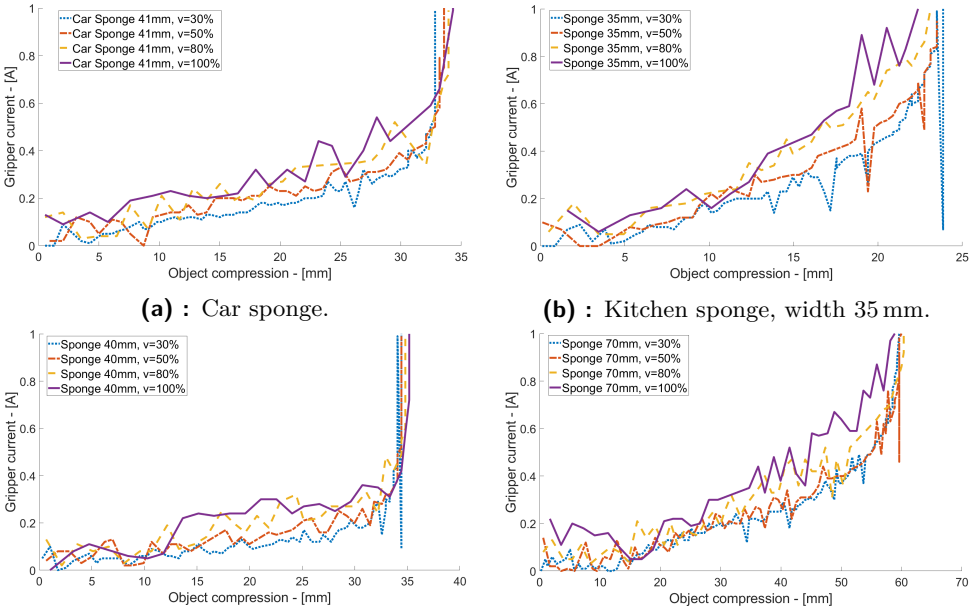


**(a) :** Car sponge.

**(b) :** Kitchen sponge, width 35 mm.

**(c) :** Kitchen sponge, width 40 mm.

**(d) :** Kitchen sponge, width 70 mm.

**Figure 4.17:** Overview of different closing speeds affecting the Robotiq 2F-85 gripper measurements, when gripping various sponges.

### 4.3.2 Polyurethane foams set

The next figures 4.18 to 4.21 show the results of measurements on the polyurethane foams dataset. The dataset is split into 4 groups based on the first character of the material name. The groups are

- RP type of materials, 7 objects, (see Figure 4.18)
- RL and N types of materials, 5 objects, (see Figure 4.19)
- T type of materials, 4 objects, (see Figure 4.20)
- GV and V types of materials, 4 objects, (see Figure 4.21)

The results of every material group measured by every gripper and the force/torque sensor are structured in a $4 \times 4$ array so the reader can simply compare between them. A summary of the experimentally found Young moduli is presented at the end of this section in Table 4.9. The relations of force and object compression were modified into a relation of stress and strain (see Equation 3.3), the Equation 3.7 was used and the Young modulus for each material was computed (for more information see Section 3.5). The Young modulus was measured for the close neighbourhood of object compression of 40 % (corresponds to a strain of 0.4). Where this was not possible (for the FT sensor with some objects), no values are reported. For the Robotiq 2F-85 gripper, which provides current (A) rather than force (N) feedback, the conversion outlined in Section 4.2.3 was used. Additionally, the compression speed reported is the nominal value with the empty gripper (see Table 4.4). These values are thus to be interpreted with caution. For the OnRobot RG6 gripper, continuous squeezing was not possible (see Section 3.1.3) and hence no gripping speed is reported.

### RP type materials

The resulting stress/strain relations for RP (Richfoam polyether) type materials are shown in the Figure 4.18 and the computed Young moduli listed in Table 4.5.

| Object name | OnRobot RG6 | Robotiq 2F-85 | Robotiq FT 300 |
|---|---|---|---|
| RP17**25** | 47.6 | 43.9 | 3.42 |
| RP24**40** | 88.8 | 182.3 | 8.9 |
| RP27**045** | 66.9 | 100.0 | 7.2 |
| RP30**048** | 59.0 | 106.7 | 6.5 |
| RP35**55** | 96.0 | 127.23 | 11.1 |
| RP28**65** | 248.3 | 349.8 | – |
| RP50**80** | 310.2 | 250.2 | – |

**Table 4.5:** Computed Young moduli in kPa for the RP type materials (at strain of $40\,\% \pm 5\,\%$). The materials are listed based on the compression stress values (in bold) obtained from the manufacturer. (Equation 3.7 from Section 3.5 was used for the computation.)

From the relation of the RP1725 material in all the graphs is apparent that this material is the softest, which corresponds with the compression stress value stated by the manufacturer. The computed Young moduli of this material (listed in Table 4.5) can be evaluated as the softest in all the

cases. The results for the RP2440, RP27045, RP30048 and RP3555 materials are very close to each other, which is in terms with the deviation of ±15 % denoted by the manufacturer. In the case of the OnRobot RG6 gripper and Robotiq FT 300 sensor, the RP2440 material seems to be stiffer than RP27045 and RP30048. The RP3555 is correctly distinguished as the third most stiff material in this subset. In the case of the Robotiq 2F-85 gripper, the RP2440 material is categorized as stiffer than the RP3555 material as well. The last two materials have very similar relations, however their stiffness evaluation is switched in comparison to the stated compression stress values. This is in correspondence with the force/torque sensor output. The output from the qbrobotics SoftHand is the most problematic, but the most and least stiff materials are evaluated correctly. The computed Young moduli are shown in the Table 4.5. As the materials have nonlinear properties the values vary greatly among the individual setup, however the ordering is consistent.

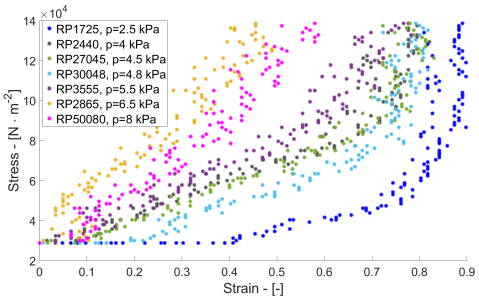


**(a) :** OnRobot RG6 gripper.

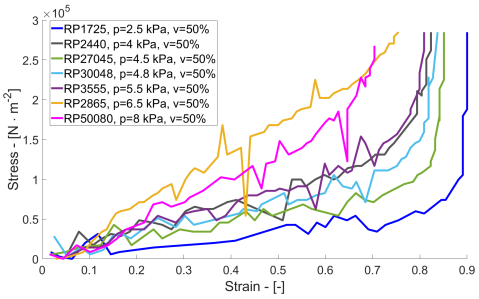


**(b) :** Robotiq 2F-85 gripper, nominal closing speed 79 mm · s$^{-1}$.

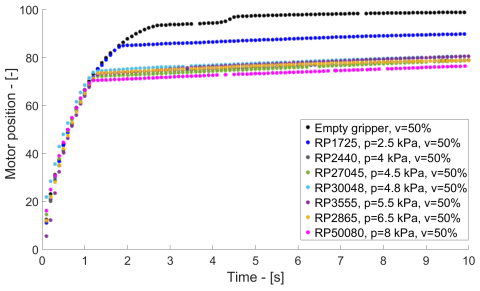


**(c) :** qbrobotics SoftHand gripper, closing speed 50 %.

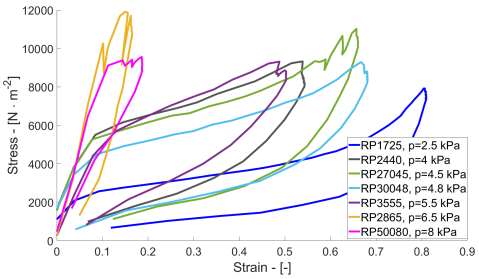


**(d) :** Robotiq FT 300 force/torque sensor, closing speed 30 mm · s$^{-1}$ and releasing speed 60 mm · s$^{-1}$.

**Figure 4.18:** Overview of strain/stress plots for RP polyurethane materials while being compressed using different grippers.

## RL and N type materials

The resulting stress/strain relations for materials of type RL and type N are shown in the Figure 4.19. The computed Young moduli are shown in the Table 4.6.

The relations do not correspond to the compression stress values stated by the manufacturer. It is difficult to identify the material with incorrectly

| Object name | OnRobot RG6 | Robotiq 2F-85 | Robotiq FT 300 |
|---|---|---|---|
| RL35**29** | 59.8 | 17.7 | 5.3 |
| NF21**40** | 97.6 | 137.0 | 4.4 |
| RL40**40** | 85.8 | 84.6 | 10.5 |
| RL50**45** | 159.1 | 193.6 | – |
| N40**72** | 131.8 | 173.0 | – |

**Table 4.6:** Computed Young moduli in kPa for the RL and N type materials (at strain of $40\,\% \pm 5\,\%$). The materials are listed based on the compression stress values (in bold) obtained from the manufacturer. (Equation 3.7 from Section 3.5 was used for the computation.)

stated value. Especially the RL5045 and N4072 materials, should have very different results as the compression stress value difference is high. However, the relations are very similar. Which is confirmed by the Robotiq FT 300 force/torque sensor. The results of the RG gripper and the Robotiq 2F-85 gripper are very analogous. The qbrobotics SoftHand is able to evaluate the supposedly softest material RL3529. The nonlinear properties are evident from the graphs, the results of the Robotiq FT 300 are not ordered consistently with the other setups.

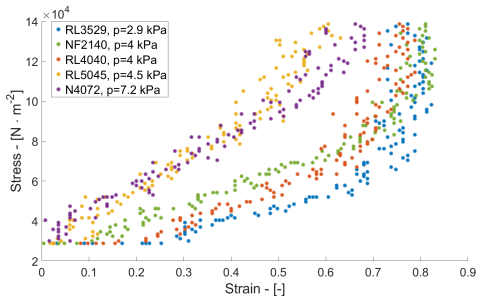


**(a) :** OnRobot RG6 gripper.

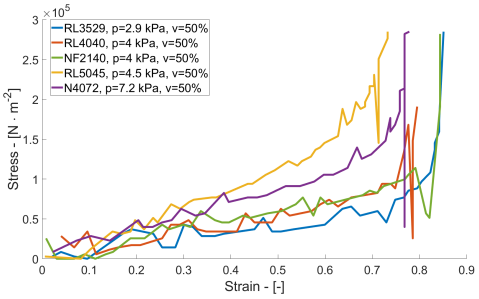


**(b) :** Robotiq 2F-85 gripper, nominal closing speed $79\,\mathrm{mm} \cdot \mathrm{s}^{-1}$.

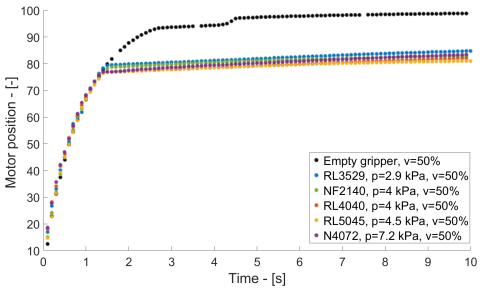


**(c) :** qbrobotics SoftHand gripper, closing speed 50 %.

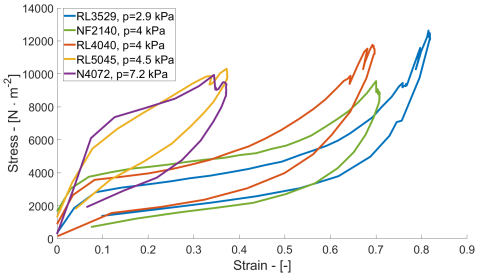


**(d) :** Robotiq FT 300 force/torque sensor, closing speed $30\,\mathrm{mm} \cdot \mathrm{s}^{-1}$ and releasing speed $60\,\mathrm{mm} \cdot \mathrm{s}^{-1}$.

**Figure 4.19:** Overview of results for RL and N polyurethane materials.

### T type materials

The resulting stress/strain relations for type T materials are shown in the Figure 4.20 and the computed Young moduli in the Table shown 4.7.

| Object name | OnRobot RG6 | Robotiq 2F-85 | Robotiq FT 300 |
|---|---|---|---|
| T18**20** | 82.8 | 106.2 | 5.5 |
| T20**30** | 105.0 | 142.3 | 3.3 |
| T32**40** | 165.0 | 166.3 | 4.4 |
| T25**45** | 321.6 | 175.0 | – |

**Table 4.7:** Computed Young moduli in kPa for the T type materials (at strain of $40\,\% \pm 5\,\%$). The materials are listed based on the compression stress values (in bold) obtained from the manufacturer. (Equation 3.7 from Section 3.5 was used for the computation.)

The relative elasticity for each material can be clearly distinguished according to their mechanical response, as in most cases, the response curves are well spread out. The trends for the OnRobot RG6 gripper and the Robotiq 2F-85 gripper are very alike, showing slight exponential growth rate. All the grippers (including the qbrobotics SoftHand) demonstrate the same order of the response curves in the plots, from the softest one (T1820) to the most stiff ones (T2545). However the computed Young moduli are not consistent. The Robotiq FT 300 evaluated the T1820 material as stiffer than the T3240, which is only valid for the close neighbourhood of the chosen strain value ($40\,\%$).

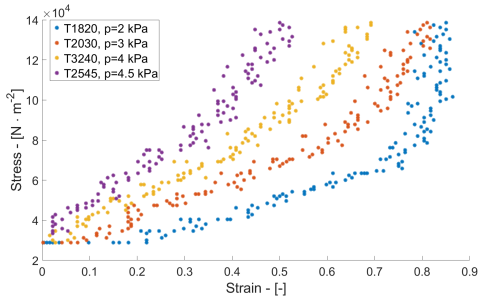


**(a) :** OnRobot RG6 gripper.

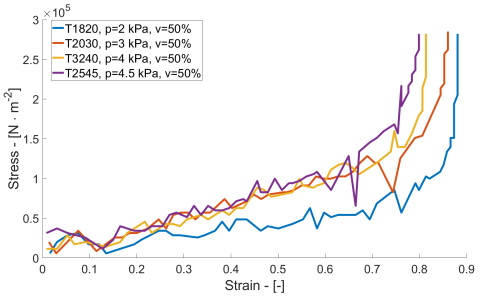


**(b) :** Robotiq 2F-85 gripper, nominal closing speed 79 mm · s$^{-1}$.

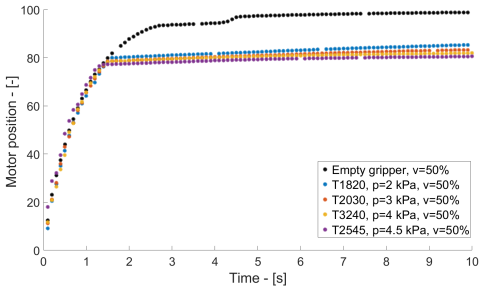


**(c) :** qbrobotics SoftHand gripper, closing speed 50 %.

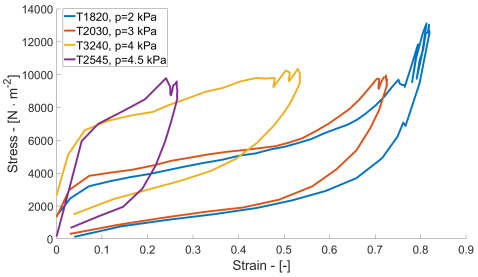


**(d) :** Robotiq FT300 force/torque sensor, closing speed 30 mm · s$^{-1}$ and releasing speed 60 mm · s$^{-1}$.

**Figure 4.20:** Overview of results for T polyurethane materials.

## V and GV type materials

The resulting stress/strain relations for materials of type V and type GV are shown in the Figure 4.21 and the computed Young moduli are shown in the Table 4.8.

| Object name | OnRobot RG6 | Robotiq 2F-85 | Robotiq FT 300 |
|---|---|---|---|
| V45**15** | 63.6 | 43.5 | 13.8 |
| V50**15** | 33.5 | 35.6 | 4.6 |
| GV50**30** | 51.5 | 87.3 | 7.4 |
| GV50**40** | 126.7 | 350.5 | – |

**Table 4.8:** Computed Young moduli in kPa for the V and GV type materials (at strain of 40 % ± 5 %). The materials are listed based on the compression stress values (in bold) obtained from the manufacturer. (Equation 3.7 from Section 3.5 was used for the computation.)

The GV5040 can be determined as the hardest material out of the group which is in agreement with the compression stress value stated by the manufacturer. Its relation is almost linear (evident in the case of the Robotiq 2F-85 gripper). The expected compression stress value of the V4515 does not seem to correspond with the results. The computed Young moduli for this material are higher (in 2 of the 3 cases) than the GV5030 material (supposed to have 2 times higher compression stress value). The V5015 is correctly distinguished

as the least stiff material in all the cases. However, the trend for the GV5030 was expected to have a similar relation as the GV5040 which is not the case. The response curves from the force/torque sensor are in correspondence with the other relations.

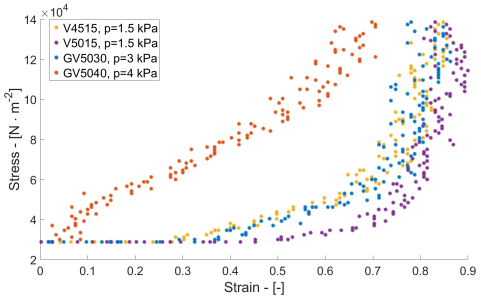


**(a) :** OnRobot RG6 gripper.

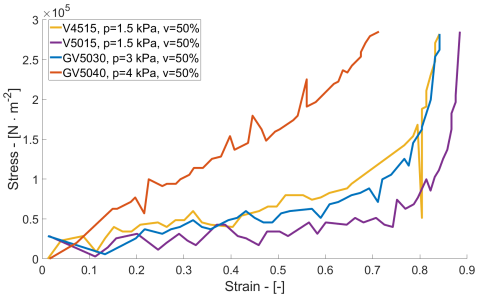


**(b) :** Robotiq 2F-85 gripper, nominal closing speed $79\,\mathrm{mm} \cdot \mathrm{s}^{-1}$.

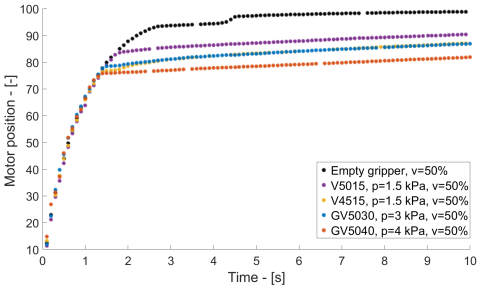


**(c) :** qbrobotics SoftHand gripper, closing speed 50 %.

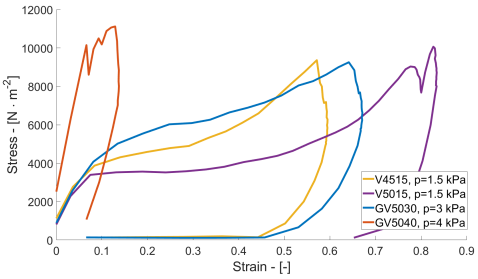


**(d) :** Robotiq FT300 force/torque sensor, closing speed $30\,\mathrm{mm} \cdot \mathrm{s}^{-1}$ and releasing speed $60\,\mathrm{mm} \cdot \mathrm{s}^{-1}$.

**Figure 4.21:** Overview of results for V and GV polyurethane materials.

| Object name | OnRobot RG6 | Robotiq 2F-85 | Robotiq FT 300 |
|---|---|---|---|
| T25**45** | 321.6 | 175.0 | – |
| RP500**80** | 310.2 | 250.2 | – |
| RP28**65** | 248.3 | 349.8 | – |
| T32**40** | 165.0 | 166.3 | 4.4 |
| RL50**45** | 159.1 | 193.6 | – |
| N40**72** | 131.8 | 173.0 | – |
| GV50**40** | 126.7 | 350.5 | – |
| T20**30** | 105.0 | 142.3 | 3.3 |
| NF21**40** | 97.6 | 137.0 | 4.4 |
| RP35**55** | 96.0 | 127.23 | 11.1 |
| RP24**40** | 88.8 | 182.3 | 8.9 |
| RL40**40** | 85.8 | 84.6 | 10.5 |
| T18**20** | 82.8 | 106.2 | 5.5 |
| RP2704**5** | 66.9 | 100.0 | 7.2 |
| V45**15** | 63.6 | 43.5 | 13.8 |
| RL35**29** | 59.8 | 17.7 | 5.3 |
| RP3004**8** | 59.0 | 106.7 | 6.5 |
| GV50**30** | 51.5 | 87.3 | 7.4 |
| RP17**25** | 47.6 | 43.9 | 3.4 |
| V50**15** | 33.5 | 35.6 | 4.6 |

**Table 4.9:** A summary of the experimentally found Young moduli of polyuerthane foams (at strain of 40 % ± 5 %), sorted according to the values found by the OnRobot RG6 gripper.

### 4.3.3 Cubes and dice set

In this section the results for the cubes and dice set (see Section 4.1.3 are presented. The set is shown in the Figure 4.22 for an illustration.

**Figure 4.22:** Set of cubes.

The resulting stress/strain relations are shown in Figure 4.23 and are again structured in a 4 × 4 array. The computed Young moduli are shown in the Table 4.10. The Young modulus was measured for the close neighbourhood of object compression of 10 % (corresponds to a strain of 0.1). Where this was not possible no values are reported.

| Object name | OnRobot RG6 | Robotiq 2F-85 | Robotiq FT 300 |
|---|---|---|---|
| Darkblue die | – | 4,023.4 | 54.9 |
| Kinova cube | 1,028.0 | 336.1 | 45.1 |
| White die | 1,235.3 | 796.6 | 43.8 |
| Pink die | 977.0 | 654.7.5 | 43.0 |
| Blue die | 28.5 | 48.8 | 7.3 |
| Yellow cube | 134.2 | 227.8.6 | 4.3 |
| Blue cube | 0.0 | 36.9 | 0.9 |

**Table 4.10:** Computed Young moduli in kPa for the Cubes and Dice set (at strain of $10\,\% \pm 5\,\%$), sorted according to the values found by the force/torque sensor. (Equation 3.7 from Section 3.5 was used for the computation.)

The darkblue die is the most stiff object out of the set. Blue cube and blue die are made out of the same material and even though they have a different size, they are distinguished as very soft in all the cases. Both objects from the light blue material have the final compression of over $80\,\%$ of the original width. The yellow cube is evaluated as softer than the blue die by the Robotiq FT 300. However, that is not the case for the other 2 grippers, as the yellow cube is evaluated as soft but not softer than the blue die. The trends for the yellow cube, blue cube and blue die exhibit nonlinear trends similar to the ones from the polyurethane foams set (for both the OnRobot RG6 and the Robotiq 2F-85 grippers). The rest of the dies have fairly linear relations. The qbrobotics SoftHand correctly distinguished the blue cube and blue die. However a result of a slipped finger disrupted the relation for the pink die. The darkblue die, having very small dimensions to be grasped with all the fingers, is also identified incorrectly.

**Squeezing with different speeds.** To give an idea of the effect of various gripping speeds, the relation of different speeds is shown in Figure 4.24, when using the 2F-85 gripper. The difference is not very apparent as the plotlines are relatively similar, only the slope varies slightly.

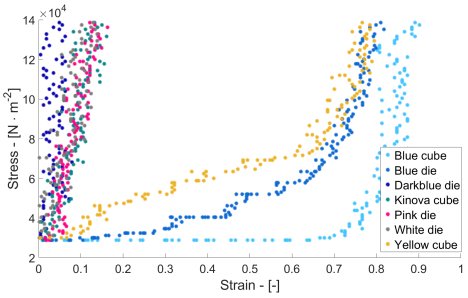


**(a) :** OnRobot RG6 gripper.

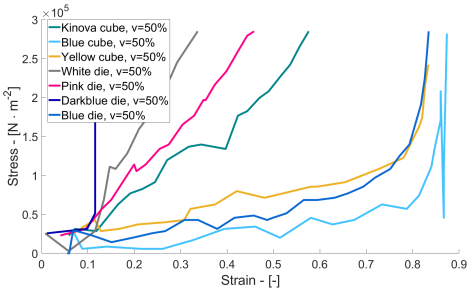


**(b) :** Robotiq 2F-85 gripper, nominal closing speed $79\,\mathrm{mm} \cdot \mathrm{s}^{-1}$.

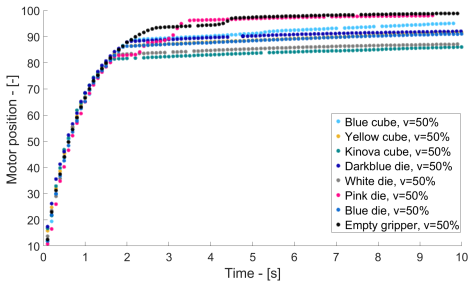


**(c) :** qbrobotics SoftHand gripper, closing speed 50 %.

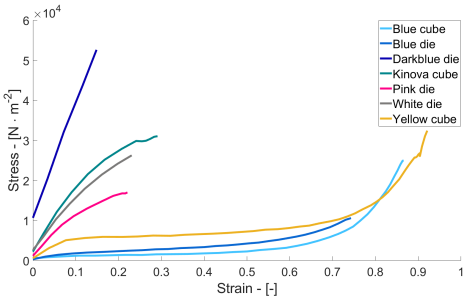


**(d) :** Robotiq FT300 force/torque sensor, closing speed $30\,mm \cdot s^{-1}$.

**Figure 4.23:** Overview of results for the Cubes and dice set while being squeezed with different grippers.

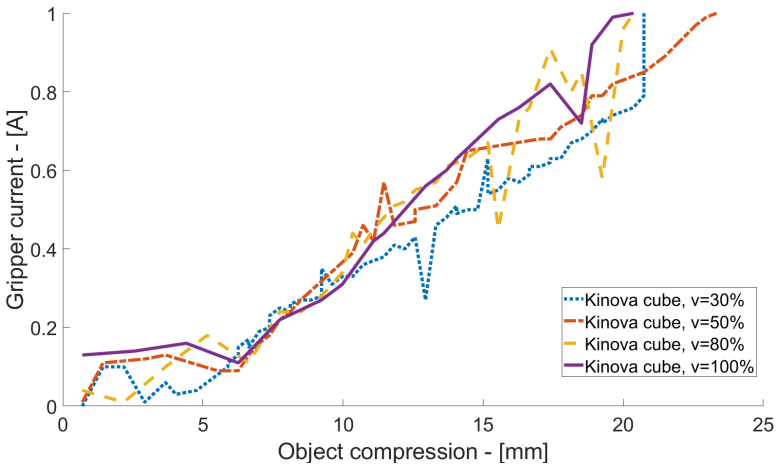


**Figure 4.24:** Comparison of different speeds of the Robotiq 2F-85 gripper, when gripping the Kinova Cube. (See Table 4.4 for the nominal closing speeds in $\mathrm{mm} \cdot \mathrm{s}^{-1}$.)

# Chapter 5

# Conclusion

In this thesis, research on exploring object material properties with robotic grippers is presented. Stiffness of various objects—or elasticity of the materials they are composed of—was explored by compressing them with a rich set of different grippers/robot hands. First, a pilot set of 13 everyday objects with an emphasis on soft/deformable objects was formed. The set consists of mainly various sponges, toys, dice and objects for squeezing (like stress ball). The pilot set was used for exploring the gripper feedback capabilities, measuring methods and to select the most suitable object candidates for the experiments. Objects made from homogeneous material and cuboid shape were preferred. To test the difference in size, the objects of the same material but different dimensions were acquired.

Then, two additional sets of materials for further experiments were assembled. The first set was formed out of 20 blocks of polyurethane foams of different properties, provided by Libea, s.r.o. distributor. The second set contains 4 dice and 3 cubes. The cubes were cut to the same dimensions. The materials from the polyurethane foam set are subject to ISO certification and the manufacturer states the material properties (including the compression stress value) in the respective technical specification. To obtain additional reference measurements, also for the cubes and dice, collaboration was established with experts at the Faculty of Mechanical Engineering, FEE, CTU, but the epidemic situation did not make it possible to perform these measurements before thesis submission.

For stiffness/elasticity exploration, the following 3 robotic grippers were used:

- The OnRobot RG6 gripper;
- The Robotiq 2F-85 gripper;
- The qbrobotics SoftHand.

Programs for measurements during object squeezing and output data logging were implemented for each gripper. Additionally, the Robotiq FT 300 force/torque sensor was also employed. For the case of the Robotiq 2F-85 gripper the ROS Kortex driver functions were used for the gripper control and communication. A custom ROS package was developed as an extension

to the driver, a ROS node from this package was used to receive and log the gripper feedback. Another custom ROS node was implemented for a subscription to the topics published by the respective qbrobotics SoftHand ROS nodes and their logging. For the OnRobot RG6 gripper and Robotiq FT 300 F/T sensor, the Universal Robots Polyscope interface was used. Custom gripping programs that send the measurements via the Ethernet connection were implemented in this interface using the URScript programming language. The implemented source codes were uploaded to the Gitlab directory [33] to its respective folders.

Both sets of materials were explored with each of the grippers multiple times and with various settings. The relation of the gripping force and the object compression was measured with the OnRobot RG6 gripper. The relation of the gripper current and the object compression was measured with the Robotiq 2F-85 gripper, using 3 closing speed settings. The relation of the gripper current and the gripper position was measured with the qbrobotics SoftHand, using 3 closing speed settings. However, for discriminating objects of different stiffness, a plot of motor position over time was found to be better suited. The relation of force and the object compression was also measured with the Robotiq FT 300 force/torque sensor (one speed of compression). The data from the measurements are saved on the Google Drive [77] in the `Data` folder. Some of the measurements were also recorded and the videos are included in the `Videos` folder.

For each gripper, the relations were plotted and examined. A special MATLAB function for fast plotting of the data was implemented. Selected relations were presented in the results (see Chapter 4). Young moduli were computed for the gripper outputs with the exception of the SoftHand. From the plots the relative stiffness can be determined as the slopes of mechanical response curves differ for each material: more elastic materials can be distinguished from less elastic ones. The relative ordering by stiffness/elasticity using the grippers corresponds with the force/torque sensor output. However, in absolute terms, the Young moduli obtained are not precise and vary greatly among the grippers. For the foam set, the values do not match with the compression stress value from the data sheet. The source code is uploaded to a gitlab directory [33] to the `MATLAB\_functions` folder.

The OnRobot RG6 gripper exhibits consistent results, but the gripper width measurement is noisy, the closing speed is slow and the control options are limited. The Robotiq 2F-85 gripper offers great control options, but the feedback resolution is low and unsatisfactory. The qbrobotics SoftHand is not ideal for this kind of experiment, as it lacks precision. However, it can provide some value, even though the process is time consuming. None of the grippers are suitable for precise stiffness/elasticity estimation, but they can be used to discriminate objects based on their relative stiffness. The force/torque sensor is a good addition to the grippers and can produce very clean mechanical response curves. However, the UR10e manipulator, on which the sensor was mounted, did not allow compression forces greater than 100 N which limited the object/material exploration via squeezing.

# Chapter 6

# Discussion and future work

## 6.1 OnRobot RG6 gripper

The OnRobot RG6 is a capable industrial gripper but for haptic exploration its capabilities are slightly limited. The URCap control provides useful functionality but it is still not ideal. The gripper offers a grip detection, measures the width between the gripper fingertips and can detect if the gripping force was reached. There is also a depth compensation feature which enables the fingers to sweep in a straight horizontal line. However these functions were not very helpful during the research. The control of the gripper is not precise enough, the smallest unit is a mm. The feedback is not continuous; in other words, the gripper cannot move and monitor the gripping force at the same time and the width measurement is very noisy. During this research, I found an alternative way to control the gripper—probably unintended by the manufacturer.

The gripper should work sufficiently in an industrial environment. The use case is more suited for manipulation of solid and stiff objects, ideally with a known size. The gripper can easily detect the grasp and the objects can be then sorted based on the measured width. The same could be achievable with the soft objects but the whole process would lack the needed precision to be truly reliable. It is possible for the gripper to distinguish between the objects and sort them based on their stiffness but only in comparison to each other. Maybe a different gripping routine composed of multiple grasps and re-grasps with varying gripping forces could be more successful. Also a differently shaped pair of fingertips can affect the results.

## 6.2 Robotiq 2F-85 gripper

Thanks to the ROS Kortex driver, the Robotiq 2F-85 gripper mounted on a Kinova Gen3 manipulator is very simple to work with and the setup is quick and straightforward. This user friendliness could be considered as the main advantage of the gripper. The driver offers a good control of the gripper with its two control modes (position and velocity). Unfortunately, the force control, which the gripper should be capable of, has not been implemented yet. There

is an option of developing a custom gripping program that would control the gripper via the RS-485 interface, but that would be time consuming and out of the scope of this thesis. The Robotiq 2F-85 provides a sufficient feedback about its state. Values like position, motor current, voltage and temperature can be logged. The problem is that the resolution of the sensors is not adequate and with the higher logging frequency, the sensors are not capable of providing relevant data. Moreover, the gripper does not provide the gripping force measurement. From the results, the motor current seems to be analogous to the gripping force. The maximum gripping force is the highest out of the three grippers. The gripper fingertips can be also modified.

## 6.3 qbrobotics SoftHand

The qbrobotic SoftHand has a very simple and interesting design. It is capable of grasping and picking up everyday objects. It can be also used for pushing buttons, opening doors and other simple tasks. The SoftHand only uses one motor for closing and opening. The closing speed and gripper closure can be set, but the feedback is very limited. There is no proprioceptive feedback as such, only the output from the motor encoder and the motor current can be measured. From the results, the stiffness is hard to determine. To utilize the SoftHand to its full potential a tactile skin on the fingertips could be equipped. Another possibility would be to utilize the Robotiq FT 300 force/torque sensor with the SoftHand and record the forces and torques when stroking the surfaces of the materials.

## 6.4 Results

Unfortunately, the properties of the materials were not tested on a proper measuring device in time. Therefore, reference values were only available for the polyurethane foam set. However, the measurements obtained for each gripper are mostly coherent in terms of relative ordering of the objects/ materials by their stiffness/elasticity. This holds also for the compression using the force/torque sensor. Best results—based on relative correspondence with the compression stress value from the data sheet—were obtained for the T type polyurethane foams. This could be exploited as a kind of baseline and all the other materials could be organized based on those values. The problem is, that this is only relative estimation based on the order of elasticity values/-gradients of response curves. Therefore, the grippers can assess the stiffness of the object only relatively, but it can be still used for object discrimination. The RG6 gripper and the 2F-85 gripper can be definitely used for an object classifier based on the object stiffness. Another goal would be to use the robotic setups to group the objects based on how stiff they are in a real time. Various classifier models can be used e.g. neural networks, SVM, random forests, etc.

## 6.5 Future work

In the future several concepts would be worth pursuit, such as:

- Exploration of the Young modulus along the whole response curve, not just one close area.
- Preconditioning of the material – by gripping and releasing multiple times.
- Utilization of the force/torque sensor more in tandem with the grippers, for poking, scratching and sweeping.
- Examination of effects of different custom fingertips.
- Model approximation of the deformable objects based on the measurements, similar to [13] and [78].
- Exploration of a wider variety of object shapes.
- Training and evaluation of a classifier on the dataset.

# Bibliography


[1] J. Dargahi and S. Najarian, "Advances in tactile sensors design/manufacturing and its impact on robotics applications–a review," *Industrial Robot: An International Journal*, 2005.

[2] A. Jimenez and B. M. Al Hadithi, *Robot Manipulators: Trends and Development*. BoD–Books on Demand, 2010.

[3] "Sense Of Touch: discover how skin makes our sense of touch possible," Billings, 2017-2020, accessed: 2020-04-01. [Online]. Available: https://learning-center.homesciencetools.com/article/skin-touch/#sense

[4] G. H. Büscher, R. Kõiva, C. Schürmann, R. Haschke, and H. J. Ritter, "Flexible and stretchable fabric-based tactile sensor," *Robotics and Autonomous Systems*, vol. 63, pp. 244 – 252, 2015. [Online]. Available: http://www.sciencedirect.com/science/article/pii/S0921889014001821

[5] A. Schmitz, P. Maiolino, M. Maggiali, L. Natale, G. Cannata, and G. Metta, "Methods and technologies for the implementation of large-scale robot tactile sensors," *IEEE Transactions on Robotics*, vol. 27, no. 3, pp. 389–400, 2011.

[6] S. Teshigawara, S. Shimizu, K. Tadakuma, M. Aiguo, M. Shimojo, and M. Ishikawa, "High sensitivity slip sensor using pressure conductive rubber," in *SENSORS, 2009 IEEE*, 2009, pp. 988–991.

[7] "The Interactive Perception-Action-Learning for Modelling Objects (IPALM) project," 2020. [Online]. Available: https://sites.google.com/view/ipalm/home

[8] B. Calli, A. Singh, J. Bruce, A. Walsman, K. Konolige, S. Srinivasa, P. Abbeel, and A. M. Dollar, "Yale-cmu-berkeley dataset for robotic manipulation research," *The International Journal of Robotics Research*, vol. 36, no. 3, pp. 261–268, 2017.

[9] S. Luo, J. Bimbo, R. Dahiya, and H. Liu, "Robotic tactile perception of object properties: A review," *Mechatronics*, vol. 48, pp. 54–67, 2017.

[10] J. Bohg, K. Hausman, B. Sankaran, O. Brock, D. Kragic, S. Schaal, and G. S. Sukhatme, "Interactive perception: Leveraging action in perception and perception in action," *IEEE Transactions on Robotics*, vol. 33, no. 6, pp. 1273–1291, 2017.

[11] R. Klatzky and C. L. Reed, "Haptic exploration," *Scholarpedia*, vol. 4, no. 8, p. 7941, 2009, revision #150489.

[12] B. Frank, R. Schmedding, C. Stachniss, M. Teschner, and W. Burgard, "Learning the elasticity parameters of deformable objects with a manipulation robot," in *2010 IEEE/RSJ International Conference on Intelligent Robots and Systems*. IEEE, 2010, pp. 1877–1883.

[13] B. Frank, C. Stachniss, R. Schmedding, M. Teschner, and W. Burgard, "Learning object deformation models for robot motion planning," *Robotics and Autonomous Systems*, vol. 62, no. 8, pp. 1153–1174, 2014.

[14] P. Boonvisut and M. C. Çavuşoğlu, "Estimation of soft tissue mechanical parameters from robotic manipulation data," *IEEE/ASME Transactions on Mechatronics*, vol. 18, no. 5, pp. 1602–1611, 2012.

[15] M. C. Gemici and A. Saxena, "Learning haptic representation for manipulating deformable food objects," in *2014 IEEE/RSJ International Conference on Intelligent Robots and Systems*. IEEE, 2014, pp. 638–645.

[16] K. Takahashi and J. Tan, "Deep visuo-tactile learning: Estimation of tactile properties from images," in *2019 International Conference on Robotics and Automation (ICRA)*, 2019, pp. 8951–8957.

[17] A. Tulbure and B. Bäuml, "Superhuman performance in tactile material classification and differentiation with a flexible pressure-sensitive skin," in *2018 IEEE-RAS 18th International Conference on Humanoid Robots (Humanoids)*. IEEE, 2018, pp. 1–9.

[18] M. Strese, J.-Y. Lee, C. Schuwerk, Q. Han, H.-G. Kim, and E. Steinbach, "A haptic texture database for tool-mediated texture recognition and classification," in *2014 IEEE International Symposium on Haptic, Audio and Visual Environments and Games (HAVE) Proceedings*. IEEE, 2014, pp. 118–123.

[19] J. Bednarek, M. Bednarek, P. Kicki, and K. Walas, "Robotic touch: Classification of materials for manipulation and walking," in *2019 2nd IEEE International Conference on Soft Robotics (RoboSoft)*. IEEE, 2019, pp. 527–533.

[20] M. Kerzel, E. Strahl, C. Gaede, E. Gasanov, and S. Wermter, "Neuro-robotic haptic object classification by active exploration on a novel dataset," in *2019 International Joint Conference on Neural Networks (IJCNN)*, 2019, pp. 1–8.

[21] M. Hoffmann, K. Štěpánová, and M. Reinstein, "The effect of motor action and different sensory modalities on terrain classification in a quadruped robot running with multiple gaits," *Robotics and Autonomous Systems*, vol. 62, no. 12, pp. 1790–1798, 2014.

[22] T. Bhattacharjee, J. M. Rehg, and C. C. Kemp, "Haptic classification and recognition of objects using a tactile sensing forearm," in *2012 IEEE/RSJ International Conference on Intelligent Robots and Systems*. IEEE, 2012, pp. 4090–4097.

[23] A. J. Spiers, M. V. Liarokapis, B. Calli, and A. M. Dollar, "Single-grasp object classification and feature extraction with simple robot hands and tactile sensors," *IEEE transactions on haptics*, vol. 9, no. 2, pp. 207–220, 2016.

[24] C. Hellmann, A. Bajrami, and W. Kraus, "Enhancing a robot gripper with haptic perception for risk mitigation in physical human robot interaction," in *2019 IEEE World Haptics Conference (WHC)*, 2019, pp. 253–258.

[25] L. Chin, J. Lipton, M. C. Yuen, R. Kramer-Bottiglio, and D. Rus, "Automated recycling separation enabled by soft robotic material classification," in *2019 2nd IEEE International Conference on Soft Robotics (RoboSoft)*, 2019, pp. 102–107.

[26] Z. Samadikhoshkho, K. Zareinia, and F. Janabi-Sharifi, "A brief review on robotic grippers classifications," in *2019 IEEE Canadian Conference of Electrical and Computer Engineering (CCECE)*. IEEE, 2019, pp. 1–4.

[27] Z. Kappassov, J.-A. Corrales, and V. Perdereau, "Tactile sensing in dexterous robot hands," *Robotics and Autonomous Systems*, vol. 74, pp. 195–220, 2015.

[28] A. Drimus, G. Kootstra, A. Bilberg, and D. Kragic, "Design of a flexible tactile sensor for classification of rigid and deformable objects," *Robotics and Autonomous Systems*, vol. 62, no. 1, pp. 3 – 15, 2014, new Boundaries of Robotics. [Online]. Available: http://www.sciencedirect.com/science/article/pii/S092188901200125X

[29] J. M. Butt, H. Wang, and R. Pathan, "Design, fabrication, and analysis of a sensorized soft robotic gripper," in *2018 IEEE 8th Annual International Conference on CYBER Technology in Automation, Control, and Intelligent Systems (CYBER)*, 2018, pp. 169–174.

[30] B. S. Homberg, R. K. Katzschmann, M. R. Dogar, and D. Rus, "Haptic identification of objects using a modular soft robotic gripper," in *2015 IEEE/RSJ International Conference on Intelligent Robots and Systems (IROS)*, 2015, pp. 1698–1705.

[31] S. A. Stansfield, "A haptic system for a multifingered hand," in *Proceedings. 1991 IEEE International Conference on Robotics and Automation*, 1991, pp. 658–664 vol.1.

[32] N. Gorges, S. Escaida Navarro, D. Göger, and H. Wörn, "Haptic object recognition using passive joints and haptic key features," in *2010 IEEE International Conference on Robotics and Automation*, 2010, pp. 2349–2355.

[33] P. Stoudek and M. Mareš, 2020. [Online]. Available: https://gitlab.fel.cvut.cz/body-schema/ipalm/ipalm-grasping

[34] "UR10e Collaborative industrial robotic arm," 2020, accessed: 2020-05-06. [Online]. Available: https://www.universal-robots.com/products/ur10-robot/

[35] "Universal Robots e-Series User Manual UR10e, version 5.8," 2020, accessed: 2020-05-06. [Online]. Available: https://s3-eu-west-1.amazonaws.com/ur-support-site/69139/99405_UR10e_User_Manual_en_Global.pdf

[36] "Universal Robots UR10e," Marion, 2020, accessed: 2020-05-05. [Online]. Available: https://www.robots.com/images/robots/Universal/Universal_UR10_0002.jpg

[37] "RG6 gripper," 2020, accessed: 2020-05-06. [Online]. Available: https://onrobot.com/en/products/rg6-gripper

[38] "RG6 Gripper Datasheet," 2017, accessed: 2020-05-06. [Online]. Available: https://www.universal-robots.com/media/1800257/rg6-gripper-datasheet.pdf

[39] "RG6 gripper," Trenčín, 2020, accessed: 2020-05-06. [Online]. Available: https://marvin-robotics.com/wp-content/uploads/rg6_gripper.jpg

[40] "FT 300 Force Torque Sensor - Robotiq," 2020, accessed: 2020-05-06. [Online]. Available: https://robotiq.com/products/ft-300-force-torque-sensor

[41] "Robotiq FT 300," 2020, accessed: 2020-05-06. [Online]. Available: https://www.amtech.cz/userfiles/products/September2018/RDdhOOZz5YRAccsdYjBB.png

[42] "Universal Robots Github repository," 2020, accessed: 2020-05-06. [Online]. Available: https://github.com/UniversalRobots

[43] "Universal Robots ROS Driver," 2020, accessed: 2020-05-06. [Online]. Available: https://github.com/UniversalRobots/Universal_Robots_ROS_Driver

[44] "Universal Robots support," 2020, accessed: 2020-05-06. [Online]. Available: https://www.universal-robots.com/support/

[45] "Dashboard Server E-Series, Port 29999," 2020, accessed: 2020-05-06. [Online]. Available: https://www.universal-robots.com/articles/ur-articles/dashboard-server-e-series-port-29999/

[46] A. Shetty, "SocketTest v3.0.0," 2008. [Online]. Available: http://sockettest.sourceforge.net

[47] "Real-Time Data Exchange (RTDE) Guide," 2020, accessed: 2020-05-06. [Online]. Available: https://www.universal-robots.com/articles/ur-articles/real-time-data-exchange-rtde-guide/

[48] "User Manual RG6 Industrial Robot Gripper," 2020, accessed: 2020-05-06. [Online]. Available: https://dev.onrobot.com/sites/default/files/documents/RG6_User_Manual_enEN_V1.9.2.pdf

[49] "FT 300 Force Torque Sensor - Instruction Manual," 2018, accessed: 2020-05-06. [Online]. Available: https://assets.robotiq.com/website-assets/support_documents/document/FT_Sensor_Instruction_Manual_PDF_20181218.pdf

[50] "TCP/IP Socket Communication via URScript," 2020, accessed: 2020-05-06. [Online]. Available: https://www.universal-robots.com/articles/ur-articles/tcpip-socket-communication-via-urscript/

[51] "The URScript Programming Language, version 5.5," 2020, accessed: 2020-05-06. [Online]. Available: https://s3-eu-west-1.amazonaws.com/ur-support-site/69271/scriptManual.pdf

[52] "Kinova Gen3 | Kinova," 2020, accessed: 2020-05-06. [Online]. Available: https://www.kinovarobotics.com/en/products/gen3-robot

[53] "Kinova Gen3," 2019, accessed: 2020-05-06. [Online]. Available: https://wevolver-project-images.s3.amazonaws.com/0.8nqj4rvsjmkimg-gallery-gen3-01.jpg

[54] "2F-85 and 2F-140 Grippers - Robotiq," accessed: 2020-05-06. [Online]. Available: https://robotiq.com/products/2f85-140-adaptive-robot-gripper

[55] "Robotiq 2F-85," Doetinchem, 2020, accessed: 2020-05-06. [Online]. Available: https://wiredworkers.io/wp-content/uploads/2019/08/Robotiq-2-Finger-85-real.png

[56] "2F-85 & 2F-140 - Instruction Manual," 2020, accessed: 2020-05-06. [Online]. Available: https://assets.robotiq.com/website-assets/support_documents/document/2F-85_2F-140_UR_PDF_20200211.pdf

[57] "ROS kortex," accessed: 2020-05-06. [Online]. Available: https://github.com/kinovarobotics/ros_kortex

[58] "ROS kortex vision," accessed: 2020-05-06. [Online]. Available: https://github.com/Kinovarobotics/ros_kortex_vision

[59] "Writing a Simple Publisher and Subscriber (C++)," accessed: 2020-05-06. [Online]. Available: https://wiki.ros.org/ROS/Tutorials/WritingPublisherSubscriber(c++)

[60] "Qb SoftHand Research - anthropomorphic robotic hand - qbrobotics," accessed: 2020-05-06. [Online]. Available: https://qbrobotics.com/products/qb-softhand-research/

[61] "Qb robotics SoftHand," Liberec, 2020, accessed: 2020-05-06. [Online]. Available: https://www.exactec.com/images/qb-hand-attack.jpg

[62] "qb SoftHand Research User Guide, version 1.0.0," 2019, accessed: 2020-05-06. [Online]. Available: https://qbrobotics.com/wp-content/uploads/2016/03/qb-SoftHand-Research-User-Guide-1.0.0.pdf

[63] "Robots/qbhand - ROS Wiki," 2018, accessed: 2020-05-06. [Online]. Available: https://wiki.ros.org/Robots/qbhand

[64] "qbrobotics Bitbucket qbdevice-api Repository," 2020, accessed: 2020-05-06. [Online]. Available: https://bitbucket.org/qbrobotics/qbdevice-api/src/production/

[65] "qbrobotics Bitbucket qbmove_simulink Repository," 2020, accessed: 2020-05-06. [Online]. Available: https://bitbucket.org/qbrobotics/qbmove-simulink/src/production/

[66] "qbrobotics Bitbucket ROS Repository," 2020, accessed: 2020-05-06. [Online]. Available: https://bitbucket.org/qbrobotics/workspace/projects/ROS

[67] "Writing a Simple Service and Client (C++)," accessed: 2020-05-06. [Online]. Available: https://wiki.ros.org/ROS/Tutorials/WritingServiceClient(c++)

[68] "Festo DHEF gripper," 2020, accessed: 2020-05-06. [Online]. Available: https://uploads.ifdesign.de/award_img_337/oex_large/283452_02_191023_festo_dhef_gripper_02.jpg

[69] "Adaptive shape gripper DHEF | Festo," 2020, accessed: 2020-05-06. [Online]. Available: https://www.festo.com/cms/nl-be_be/69457.htm

[70] M. Bednařík, *Fyzika 1*, 1st ed. Prague: Czech Technical University, 2011.

[71] H. Chlup, "Charakter ne jen biologického materiálu," 2020.

[72] L. A. Al-Zube, D. J. Robertson, J. N. Edwards, W. Sun, and D. D. Cook, "Measuring the compressive modulus of elasticity of pith-filled plant stems," *Plant methods*, vol. 13, no. 1, p. 99, 2017.

[73] J. Smardzewski, I. Grbac, and S. Prekrat, "Nonlinear mechanics of hyper elastic polyurethane furniture foams," 2008.

[74] Engineering ToolBox, "Young's Modulus - Tensile and Yield Strength for common Materials," 2003, accessed: 2020-05-17. [Online]. Available: https://www.engineeringtoolbox.com/young-modulus-d_417.html

[75] s. Libea, "Libea.cz," 2018. [Online]. Available: https://www.libea.cz

[76] "Polyether-Schaumstoffe, RP24040, RP30048," 2015, accessed: 2020-05-17.

[77] P. Stoudek, 2020. [Online]. Available: https://drive.google.com/drive/folders/16sUG-zCwCg5HIF7EbCTBqgsklw7-vOpg?usp=sharing

[78] S. Burion, F. Conti, A. Petrovskaya, C. Baur, and O. Khatib, "Identifying physical properties of deformable objects by using particle filters," in *2008 Ieee International Conference On Robotics And Automation*. IEEE, 2008, pp. 1112–1117.

# MASTER'S THESIS ASSIGNMENT

## I. Personal and study details

Student's name: **Stoudek Pavel** Personal ID number: **420335**

Faculty / Institute: **Faculty of Electrical Engineering**

Department / Institute: **Department of Cybernetics**

Study program: **Cybernetics and Robotics**

Branch of study: **Robotics**

## II. Master's thesis details

Master's thesis title in English:

**Extracting Material Properties of Objects from Haptic Exploration Using Multiple Robotic Grippers**

Master's thesis title in Czech:

**Získání vlastností materiálu skrze haptický průzkum pomocí různých robotických uchopovačů**

Guidelines:

1. Familiarization with different robotic grippers - min. 3 of the following: Robotiq 2F-85, OnRobot RG6, QB Soft Hand, Barrett Hand.
2. Pilot data collection – grasping/squeezing objects, focusing on soft/deformable materials.
3. Assess the feedback provided by different grippers (force, load / current, position, touch) and investigate to what extent can the values be transformed to physical quantities/units (Newtons, meters etc.).
4. Focus on exploring material stiffness and elasticity through controlled squeezing with various gripper configurations and speeds. If time permits, surface roughness can also be studied.
5. Strive to obtain reference values for a selection of the objects – either from literature or by using appropriate measuring apparatus.
6. Create datasets of haptic exploration of the objects; when possible, include also visual information from a camera.
7. Discuss the results and identify the limitations of individual grippers as well as their combination in discovering object material properties.

Bibliography / sources:

[1] Bednarek, J., Bednarek, M., Kicki, P., & Walas, K. (2019). Robotic Touch: Classification of Materials for Manipulation and Walking. In 2019 2nd IEEE International Conference on Soft Robotics (RoboSoft) (pp. 527-533). IEEE.
[2] Boonvisut, P., & Çavuşoğlu, M. C. (2012). Estimation of soft tissue mechanical parameters from robotic manipulation data. IEEE/ASME Transactions on Mechatronics, 18(5), 1602-1611.
[3] Frank, B., Schmedding, R., Stachniss, C., Teschner, M., & Burgard, W. (2010, October). Learning the elasticity parameters of deformable objects with a manipulation robot. In 2010 IEEE/RSJ International Conference on Intelligent Robots and Systems (pp. 1877-1883). IEEE.
[4] Hoffmann, M., Stepanova, K. & Reinstein, M. (2014), 'The effect of motor action and different sensory modalities on terrain classification in a quadruped robot running with multiple gaits', Robotics and Autonomous Systems 62, 1790-1798.
[5] Liarokapis, M. V., Calli, B., Spiers, A. J., & Dollar, A. M. (2015, September). Unplanned, model-free, single grasp object classification with underactuated hands and force sensors. In 2015 IEEE/RSJ International Conference on Intelligent Robots and Systems (IROS) (pp. 5073-5080). IEEE.
[6] Tulbure, A., & Bäuml, B. (2018, November). Superhuman Performance in Tactile Material Classification and Differentiation with a Flexible Pressure-Sensitive Skin. In 2018 IEEE-RAS 18th International Conference on Humanoid Robots (Humanoids) (pp. 1-9). IEEE.

 

Name and workplace of master's thesis supervisor:

**Mgr. Matěj Hoffmann, Ph.D., Vision for Robotics and Autonomous Systems, FEE**

Name and workplace of second master's thesis supervisor or consultant:

**Mgr. Karla Štěpánová, Ph.D., Robotic Perception, CIIRC**

Date of master's thesis assignment: **19.12.2019** Deadline for master's thesis submission: **22.05.2020**

Assignment valid until: **30.09.2021**

| Mgr. Matěj Hoffmann, Ph.D.<br>Supervisor's signature | doc. Ing. Tomáš Svoboda, Ph.D.<br>Head of department's signature | prof. Mgr. Petr Páta, Ph.D.<br>Dean's signature |
|---|---|---|

## III. Assignment receipt

The student acknowledges that the master's thesis is an individual work. The student must produce his thesis without the assistance of others, with the exception of provided consultations. Within the master's thesis, the author must state the names of consultants and include a list of references.

| . | |
|---|---|
| Date of assignment receipt | Student's signature |

 